Physics – Uspekhi **51** (3) 213 – 229 (2008)

REVIEWS OF TOPICAL PROBLEMS PACS numbers: **47.20. – k**, **47.80. – v**, 98.52.Nr

Prediction and discovery of extremely strong hydrodynamic instabilities due to a velocity jump: theory and experiments

A M Fridman

DOI: 10.1070/PU2008v051n03ABEH006470

Contents

Abstract. The theory and experimental discovery of extremely strong hydrodynamic instabilities are described, viz. the Kelvin – Helmholtz, centrifugal, and superreflection instabilities. The discovery of the last two instabilities was predicted and the Kelvin – Helmholtz instability in real systems was revised by us.

1. The classical concept of hydrodynamic instabilities in an incompressible fluid

Over the past century and a half, the class of instabilities considered in monographs on fluid dynamics has been restricted to the Kelvin – Helmholtz and Rayleigh – Taylor instabilities [1–7]. Currently, a few dozen hydrodynamic-type instabilities have been discovered in continuous media (hydrodynamic and magnetohydrodynamic media, plasmas, etc.) using either incompressible or compressible models, so that classical monographs on the mechanics of continuous media, giving such a limited description of the stability problem, are simply following tradition.[1]

According to this tradition (which, in turn, was evolved in parallel with scientific discoveries), we will start here with a physical description of the hydrodynamic instability that was revealed first — the Kelvin – Helmholtz instability [1, 2, 5, 7].

1.1 Kelvin – Helmholtz instability

Let a fluid move along the x-axis.

Figure 1 displays the stationary structures first described by Lord Kelvin in the case of an incompressible fluid [2]. The straight arrows represent the velocity field that has a gradient in the y direction. In a spatially narrow region of width $\Delta y = l$, where l is small compared to the width L of the unperturbed flow, i.e., when the inequality

$$\frac{l}{L} \ll 1 \qquad (1)$$

is valid, Lord Kelvin discovered a stationary vortical pattern — a street of vortices centered in the straight line $y = y_0$ wherein the velocity vector changes its direction to the

A M Fridman Institute of Astronomy, Russian Academy of Sciences, ul. Pyatnitskaya 48, 119017 Moscow, Russian Federation
Tel. (7-495) 951 79 93. Fax (7-495) 230 20 81
E-mail: afridman@inasan.rssi.ru
Russian Research Centre 'Kurchatov Institute', Institute of Physics of Stochastic Structures, pl. Kurchatova 1, 123182 Moscow, Russian Federation

Received 5 October 2007, revised 20 December 2007
Uspekhi Fizicheskikh Nauk **178** (3) 225 – 242 (2008)
DOI: 10.3367/UFNr.0178.200803a.0225
Translated by A V Getling; edited by A Radzig

[1] True, some books dedicated to instabilities in fluid dynamics have appeared in this country in recent years — mainly translations. However, they are addressed, as a rule, to particular specialists.

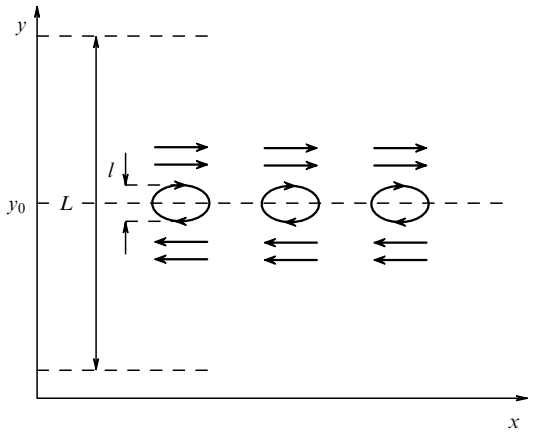

Figure 1. Velocity field in the form of stationary structures of two types. The first type is a rectilinear stream of width L with a tangential discontinuity about $y = y_0$. The second type is represented by vortices, first discovered by Lord Kelvin in 1887 and called 'cat's eyes' by him. The vortices are localized in a narrow layer of width $l \ll L$ and are centered in the straight line $y = y_0$ wherein the velocity is discontinuous and which is parallel to the x-axis.

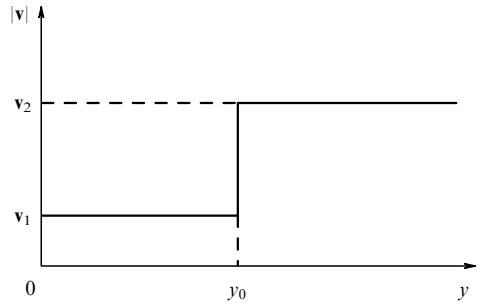

Figure 2. One-dimensional coordinate dependence of the velocity vector $\mathbf{v} = \mathbf{v}(y)$ at which the instability of the tangential discontinuity of velocity develops.

opposite one. Since the vortical pattern is, according to Ref. [2], localized in a negligibly narrow spatial domain for which $l \ll L$, the Kelvin – Helmholtz instability came later to be known as 'the instability of a tangential discontinuity of velocity', or simply 'the instability of a tangential discontinuity' (Fig. 2).

The elongated shape of such vortices, which are stretched along the x-axis (see Fig. 1), was the reason for which Lord Kelvin called them 'cat's eyes'. Each vortex contains a y-component of velocity, which, like the x-component, changes its sign near the center of the vortex; therefore, the y-component of velocity is excited in the region where the vortices are localized, while no such component is present in the remaining part of the flow.

Thus, the discovery of this vortical pattern by Lord Kelvin was also a noteworthy discovery of the first instability in fluid flows.

Under natural conditions, for example, in the Earth's atmosphere, the velocity may vary not only along the horizontal coordinate (denoted above as y) but also along the vertical coordinate, normally designated as z. At sufficiently large altitudes (usually above 10 km), a velocity inversion occurs: the velocity grows with z, sometimes reaching supersonic values.

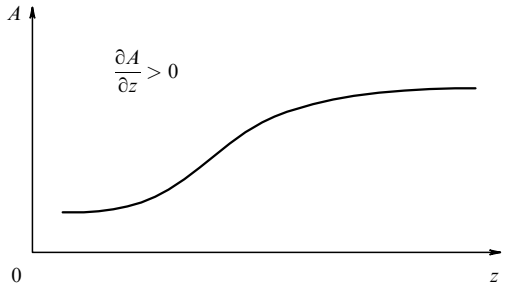

Figure 3. A dependence $A(z)$ at which the Rayleigh – Taylor instability is excited.

In the region of velocity inversion, the vector $\nabla|\mathbf{v}|$ of the velocity-magnitude gradient is collinear to the gravitational vector $\mathbf{g}$, i.e., $\mathbf{g} \parallel \nabla|\mathbf{v}|$, these two vectors being opposite in their directions. It should be noted that the velocity-inversion region in the Earth's atmosphere occurs not only at large altitudes but also near the ground surface. Indeed, the boundary condition at the Earth's surface (at $z = 0$) requires $\mathbf{v}(0) = 0$, while the inequality $\left|\mathbf{v}(z)\right| > 0$ is possible at arbitrarily small $z \neq 0$. Naturally, this does not rule out that the full velocity vector can vanish, $\mathbf{v}(x, y, z) = 0$, at various points z_i, $i = 1, 2, \ldots, n$, not only in the Earth's atmosphere but also in the ionosphere and magnetosphere.

1.2 Rayleigh – Taylor instability

In the dynamics of different continuous media, the Rayleigh–Taylor instability is known under different names related to the history of discovering this instability in each particular medium. In fluid dynamics, it is known as the instability of a heavy fluid superposed over a lighter fluid; in plasma physics, as the flute instability, etc. The development of such an instability can easily be observed if a small amount of water is poured into a glass with liquid oil. Many water flutes descending to the bottom can be seen (accordingly, the phenomenon is called the flute instability). It is obvious that the final stage of this process will be water, the heavier fluid, finding its way to the bottom of the glass, and expelling the oil upward.

Both density inversion (as in the above-considered example) and inversion in the distribution of other important parameters of the medium result in developing a similar instability. Let A be a function increasing with the density ρ, and/or temperature T, and/or pressure p, namely

$$A = A\big(\rho(z), p(z), T(z)\big)\,, \tag{2}$$

where z is the vertical coordinate which increases in the direction opposite to the direction of the gravitational vector $\mathbf{g}$. Then the condition of development of the Rayleigh–Taylor instability can be written as (Fig. 3)

$$\frac{\partial A}{\partial z} > 0\,. \tag{3}$$

The Kelvin – Helmholtz and Rayleigh – Taylor instabilities discussed above have proven to be the strongest among several dozen diverse instabilities discovered later in various continuous media. It is for this reason that only these two instabilities are considered both in old (classical) and in the most recent monographs on the mechanics of continuous media (fluid mechanics) in the chapter devoted to the physics of instabilities in these media.

Although the two above-described instabilities of a continuous (hydrodynamic) medium are distinguished among several dozen others, they are not equally important from the physicist's point of view. Indeed, the excitation condition for the Rayleigh–Taylor instability requires the presence of an inverse height distribution of at least one parameter of the medium. On the other hand, the Kelvin–Helmholtz instability requires only the presence of any, even if arbitrarily small, velocity gradient which is, as a rule, present in the atmosphere or ocean. It becomes clear from the aforesaid that the Kelvin–Helmholtz instability is much more frequent in nature than the Rayleigh–Taylor instability. Therefore, we give here our preference to the Kelvin–Helmholtz instability — first of all, to its simplest form relevant to the instability of a tangential discontinuity of velocity. In Section 1.3, we will formulate the classical problem of the physics of this instability in a compressible fluid and will present the modern explanation of its excitation and stabilization mechanisms.

1.3 Formulation of the classical instability problem for a tangential discontinuity of velocity in a compressible fluid [8, 9] and a modern explanation of the excitation and stabilization mechanisms of this instability [10, 11]. Syrovatskii's criticism [9] of the study by Landau [8] and a modified stabilization criterion for the instability of the tangential discontinuity [10, 11]

For adiabatic perturbations ($S = \text{const}$) considered in Refs [8, 9] the relationship between the enthalpy W, pressure p, and density ρ can be obtained from the equation $\mathrm{d}W = \mathrm{d}p/\rho$; for $p = A\rho^{\gamma}$, where A and γ are the constants (γ is the adiabatic exponent, $\gamma = c_p/c_V$, where c_p and c_V are heat capacities at constant pressure and volume, respectively), we arrive at

$$W = \frac{\gamma}{\gamma - 1}\, A^{1/\gamma} p^{(\gamma-1)/\gamma} = Bp^{\alpha}\,, \tag{4}$$

where

$$B \equiv \frac{\gamma}{\gamma - 1}\, A^{1/\gamma}\,, \qquad \alpha \equiv \frac{\gamma - 1}{\gamma}\,. \tag{5}$$

Thus, for any $\gamma > 1$ ($\alpha > 0$), the pressure p increases with the growth of W.

It was shown in paper [8] that the amplitude of perturbations decreases exponentially $[\sim \exp(-|z|/z_0)]$ with the distance from the plane $z = 0$ of the tangential discontinuity of velocity, i.e., with increasing $|z|$. Therefore, it is sufficient to restrict our consideration to the region $|z| < z_0$ (Fig. 4).

1.3.1 The physics of the subsonic-flow instability. Region I (over the 'hump' of the disturbance) in Fig. 4a can be regarded as the neighborhood of the critical section of a subsonic nozzle, where the flow velocity is known [12] to be maximum. Then, it follows from the Bernoulli equation for the *isentropic flow*

$$\frac{v^2}{2} + Bp^{\alpha} = \text{const}\,, \tag{6}$$

that the pressure over the hump should be minimum. This results in a further growth of the disturbance amplitude, i.e., in instability.

1.3.2 Landau's stabilization effect for a supersonic flow. Region I (over the hump) in Fig. 4b can be interpreted as the narrowing channel in a supersonic diffuser ($M \gg 1$), where, as is known [12], a shock front forms, at which the rate of the supersonic flow drops to its minimum value, i.e., to the sound speed, $v = c_0$. In this case, it follows from the general form of the Bernoulli equation

$$\frac{v^2}{2} + W = \text{const} \tag{7}$$

that the enthalpy W grows over the hump; therefore, the pressure also grows. As a result, the hump is 'pressed' back to region II. This is precisely the *stabilization effect* for the instability of the tangential discontinuity of velocity in a supersonic flow, discovered for the first time by Landau [8].[2]

If so, what is the basis for Syrovatskii's critical remark on the absence of such a stabilization effect?

1.3.3 Syrovatskii's criticism [9] of the original study by Landau [8]. In contrast to the two-dimensional flow assumed by Landau [8], we consider a three-dimensional flow, still directed along the x axis, with a tangential velocity discontinuity (Fig. 5): $v_0 = v_x\Theta(z)$, where Θ is the Heaviside function.

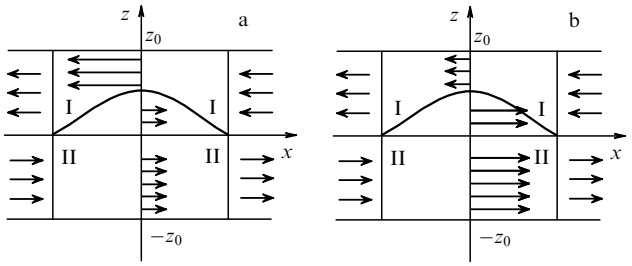

Figure 4. Perturbation of the tangential discontinuity of velocity **v** directed along the x-axis in two opposite limiting cases: (a) small Mach number $M \equiv v/c \ll 1$, or subsonic flow (c being the sound speed), and (b) $M \gg 1$, or supersonic flow.

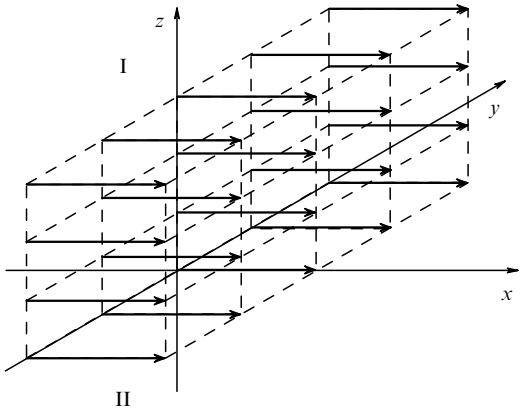

Figure 5. Three-dimensional flow directed along the x axis, with a tangential velocity discontinuity. Region I corresponds to z ($z > 0$) and Region II to z ($z < 0$).

[2] It should be noted that neither the original paper by Landau [8] nor his books coauthored by E M Lifshitz, *Mekhanika Sploshnykh Sred* (*Mechanics of Continuous Media*), 1953, 1954; and *Gidrodinamika* (*Fluid Mechanics*), 1986, give any qualitative explanation of the stabilization of the tangential-discontinuity instability for supersonic flows.

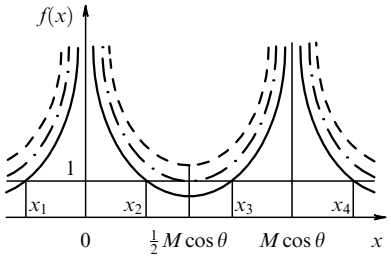

Figure 6. The function $f(x)$.

We choose three-dimensional perturbations of density, ρ_1, and velocity, v_1, in the form

$$\rho_1(x,y,z,t) = \tilde{\rho}_1 \exp\left[\mathrm{i}(k_x x + k_y y) - \lambda|z| + \gamma t\right], \qquad v_1(x,y,z,t) = \tilde{v}_1 \exp\left[\mathrm{i}(k_x x + k_y y) - \lambda|z| + \gamma t\right], \tag{8}$$

where γ is the growth rate.

Landau [8] considered the stability of the tangential discontinuity relative to two-dimensional perturbations assuming $k = k_x$, i.e., in the particular case of $k_y = 0$. He showed that, if $v_0 > v_{\mathrm{cr}}$, no instability exists for this particular class of two-dimensional perturbations. Assume that the unperturbed values of the density, ρ_0, and speed of sound, c_0, are the same on both sides of this discontinuity, i.e., $\rho_{0,\mathrm{I}} = \rho_{0,\mathrm{II}} = \rho_0$ and $c_{0,\mathrm{I}} = c_{0,\mathrm{II}} = c_0$. Then, for this very simple case, one finds

$$v_{\mathrm{cr}} = 2\sqrt{2}\, c_0 . \tag{9}$$

Ten years later, Syrovatskii [9] solved a similar problem for the general class of perturbations (8) assuming $\mathbf{k} = \{k_x, k_y\} = \{k\cos\theta, k\sin\theta\}$ (where θ is the angle between the vector $\mathbf{k}$ and its projection onto the x-axis) and revealed an instability at any v_0.

Once equalities (8) are satisfied, the problem of stability of the tangential discontinuity of the compressible-fluid velocity relative to arbitrary (but small) perturbations can be reduced to the following dispersion relation [here, the time dependence is chosen in the form $\sim \exp(-\mathrm{i}\omega t)$]:

$$k^2 c_0^2 \left[\frac{1}{(\omega - k v_0 \cos\theta)^4} - \frac{1}{\omega^4}\right] = \frac{1}{(\omega - k v_0 \cos\theta)^2} - \frac{1}{\omega^2} . \tag{10}$$

Canceling out the common factor, which has only a real root $\omega = k v_0 \cos\theta/2$, leads to the equation

$$f(x) \equiv \frac{1}{(x - M\cos\theta)^2} + \frac{1}{x^2} = 1 , \tag{11}$$

where $x \equiv \omega/(k c_0)$ and $M \equiv v_0/c_0$, which differs from the dispersion relation derived by Landau [8] by the presence of $\cos\theta$ [9]. Equation (11) has four roots. They are all real if the function $f(x)$ is similar to that shown by the solid curve in Fig. 6. If it resembles the function represented by the dashed curve in Fig. 6, Eqn (11) has two real roots. Therefore, the other two roots are complex conjugate, and one of them describes the instability. The majorant curve is dot-and-dash in Fig. 6. It corresponds to the case where all four roots are real, x_1', x_4', and $x_2' = x_3' = (1/2)M\cos\theta$, and two of them are multiple.

As can be seen from Fig. 6, the critical Mach number M_{cr} is obtained from the equation

$$f\left(\frac{1}{2} M_{\mathrm{cr}} \cos\theta\right) = 1 , \tag{12}$$

which determines the point of tangency between the majorant curve and the straight line $f(x) = 1$. This number proves to be

$$M_{\mathrm{cr}} = \frac{2\sqrt{2}}{\cos\theta} . \tag{13}$$

We use the expression for $\cos\theta = k_x/k_\perp$, where $k_\perp \equiv (k_x^2 + k_y^2)^{1/2}$, to arrive at

$$M_{\mathrm{cr}}^2 = 8\left(1 + \frac{k_y^2}{k_x^2}\right) . \tag{14}$$

In quasi-two-dimensional systems, such as the gas disks of galaxies, the rings of giant planets [13, 14], and rotating shallow water [15], only longitudinal waves considered by Landau, with $k_y/k_x \ll 1$, are possible. In this case, M_{cr} specified by Eqn (14) changes into Landau's M_{cr} [8]. According to the critical remark by Syrovatskii, arbitrary perturbations allow consideration of the opposite limiting case of transverse waves with $k_y/k_x \gg 1$. It is apparent, for example, that if

$$\frac{k_y}{k_x} \to \infty \tag{15}$$

stabilization is impossible in principle, since, as follows from Eqn (14), $M_{\mathrm{cr}} \to \infty$.[3]

1.3.4 Modified stabilization criterion for the instability of the tangential discontinuity of velocity in a compressible fluid [10, 11]. Condition (15) can be satisfied in the idealized formulation of the problem [9], which refers to a *tangential* discontinuity of velocity in *three-dimensional infinite* space. However, real situations introduce two important corrections: (1) the system has a finite spatial size in each of the three dimensions, and (2) the tangential discontinuity of velocity turns out to be smeared over a certain characteristic width a. These two conditions imply the existence of the relationship $(k_y/k_x)_{\max} \equiv (k_y)_{\max}/(k_x)_{\min}$. Indeed, $(k_x)_{\min} \sim L^{-1}$, where L is the characteristic size of the system in the x direction; the estimate $(k_y)_{\max} \sim a^{-1}$ follows from the necessary condition of the existence of an unstable flow with a nonuniform velocity profile, $k_y a < 1$ [17].

Thus, under real conditions, the instability of the tangential 'discontinuity' of velocity turns out to be quenched provided that the inequality

$$M > (M_{\mathrm{cr}})_{\mathrm{mod}} \equiv 2\left[2\left(1 + \frac{L^2}{a^2}\right)\right]^{1/2} , \tag{16}$$

holds, where $(M_{\mathrm{cr}})_{\mathrm{mod}}$ is the modified critical Mach number; if it is exceeded, no instability of the tangential discontinuity is present in a compressible fluid.

[3] It should be noted, however, that, as $k_y/k_x \to \infty$, the growth rate vanishes, $\gamma \to 0$ [16]. It can be shown that taking into account the growth of perturbations in advective flows has virtually no effect on the stabilization criterion based on formula (14).

Usually, in practice, $L^2/a^2 \gg 1$; in this case, $(M_{cr})_{mod}$ given by Eqn (16) exceeds $(M_{cr})_L$ (Landau [8]) by a factor of L/a:

$$(M_{cr})_{mod} \approx \frac{L}{a}(M_{cr})_L = \frac{L}{a}\,2\sqrt{2}\,. \tag{17}$$

We now write out the condition of advection of perturbations:

$$\frac{1}{\gamma_{max}} \gg \frac{L}{v_0}\,, \tag{18}$$

where $\gamma \equiv \mathrm{Im}\,\omega$ is the growth rate for the tangential discontinuity of velocity. The meaning of criterion (18) lies is in the fact that perturbations have no time to grow during the transit of the gas through any region of length L at the speed v_0 along the system. Indeed, the characteristic instability time described by the left-hand side of Eqn (18) far exceeds the time of gas transit through any segment of length L in the system. Thus, as condition (18) is satisfied, we can assume that no instability of tangential discontinuity is present. According to paper [16], $\gamma_{max} \approx 0.5(k_y)_{max}\,c_0 \approx 0.5(c_0/a)$, which, upon substitution into inequality (18), yields

$$M \gg 0.18(M_{cr})_{mod}\,.$$

Thus, the inequality

$$v_0 > v_{cr} \approx 0.4\sqrt{2}\,\frac{L}{a}\,c_0 \tag{19}$$

determines the stabilization criterion for the tangential discontinuity of velocity in a *real, three-dimensional compressible gas*.

2. Modern theory of tangential discontinuity and centrifugal instabilities

Since an experimental verification of the theoretical results substantially enhances their reliability, we start our presentation with a description of the experimental setups suggested by us, constructed at the Russian Research Center 'Kurchatov Institute', and used in our investigations [18–20].

2.1 The negligibly weak effect of molecular viscosity on the development mechanism of shallow-water gradient instabilities in the Spiral' setups

Our experiments were carried out using two modifications of the Spiral' setup (the second modification is shown in Fig. 7). As the working fluid, we used a green aqueous solution of $NiSO_4$, which makes it possible to obtain high-contrast photographs of spirals in red light transilluminating the solution and reflected from the white bottom of the vessel. The second modification of the setup was twice as large as the first one and consisted of two paraboloids whose shape corresponded to a shallow-water layer of a constant thickness $H_0 = 1.5-3.5$ mm, both in the core (at $\Omega_1 = 13\ \mathrm{s}^{-1}$) and at the periphery (at $\Omega_2 = 2.6\ \mathrm{s}^{-1}$).

Glycerol was added to the $NiSO_4$ solution to increase the viscosity of the solution by a factor of two to three (for all experiments in which the effect of viscosity was not intentionally studied, the total viscosity of the solution exceeded the viscosity of water by no more than 5–10 times); this addition considerably facilitated obtaining a spiral–vortex pattern at its initial formation stage. For both modifications of the setup, a rotation regime was chosen so that the radial size of the periphery, $D/2$, was much larger than the Rossby–Obukhov scale r_R (which is analogous to the characteristic Larmor radius of ions in a plasma):

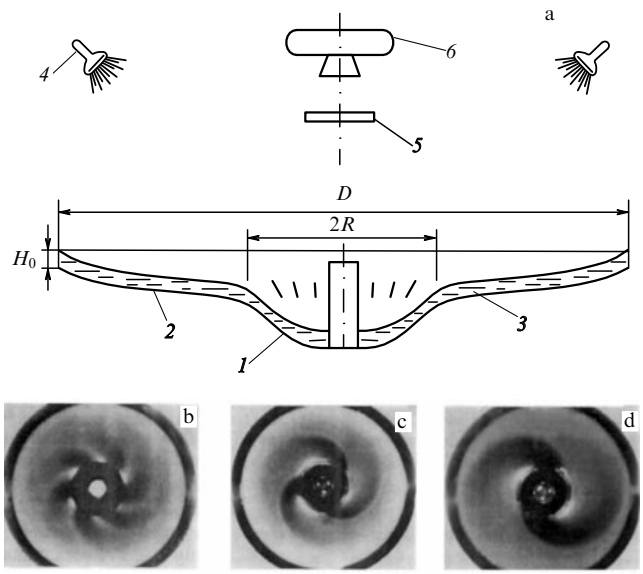

Figure 7. (a) Schematic of the Spiral' setup: *1*, core; *2*, periphery; *3*, shallow-water layer; *4*, incandescent lamps; *5*, red light filter; *6*, camera. First modification: $D = 28$ cm, the 'discontinuity' radius is $R = 4$ cm; a truncated cone whose generatrix makes an angle of 65° with the horizontal was used as the core. Second modification: $D = 60$ cm, $R = 8$ cm. The core rotates clockwise as viewed from above. (b–d) Spiral density waves generated in the shallow-water layer in the Spiral' setups by the centrifugal instability due to the velocity jump $q \equiv \Omega_2/\Omega_1$. The number of spiral arms decreases with an increase in the velocity-jump magnitude (with the decrease in the parameter q). The parameter q decreases from left to right.

$$r_R = \frac{(gH_0)^{1/2}}{2\Omega_2}\,, \tag{20}$$

where g is the gravitational acceleration. Such a choice of the regime made it possible to check whether or not the generated spirals were stable against the breakdown into vortices of size $\sim r_R$. (Notice that the chosen ratios Ω_2/Ω_1 and $r_R/(D/2)$ approach those actually measured in spiral galaxies.)

In rotating shallow water experiments, there are several numerical parameters whose magnitudes (compared to unity) determine the relative role of viscosity. First and foremost, this is the Ekman number [21]

$$E_v = \frac{v}{\Omega_0 H^2}\,, \tag{21}$$

where v is the kinematic molecular viscosity coefficient [7], Ω_0 is the angular rotational velocity of the bottom of the vessel, and H is the depth of the fluid layer. The depth H varied in the Spiral' setups from 0.2 to 0.4 cm; since $v = 0.01\ \mathrm{cm}^2\ \mathrm{s}^{-1}$ for water [18–20], we had $(E_v)_{max} \approx 1/4(\Omega_0(r))_{min}$. In experiments with a 'rotating periphery', $(\Omega_0(r))_{min} \approx 2\ \mathrm{s}^{-1}$; therefore, $(E_v)_{max} \approx 1/8$, and the viscosity effects are weak.

By definition [21], the Ekman number is $E_v \equiv \delta^2/H^2$, where $\delta = (v/\Omega_0)^{1/2}$ is the depth of the Ekman layer. Although this layer is relatively thin ($\delta^2 \ll H^2$) in our experiment, it can efficiently alter the momentum of the entire fluid layer of depth H in a certain characteristic time τ_{sp}. This is the characteristic viscous-damping time (spin

down time), or the characteristic viscous-settling time (spin up time). In our experiments [18–20], changes in the mode number were observed as the rotational velocity Ω_1 was changed abruptly, i.e., the m_1-armed spiral transformed into an m_2-armed spiral corresponding to the new rotational regime. The settling time of the new stationary regime was precisely the time τ_{sp}. Let us estimate it. To an order of magnitude, we find from the equation of motion that

$$\frac{\partial v_r}{\partial t} \sim \nu \frac{\partial}{\partial z}\left(\frac{\partial v_r}{\partial z}\right). \tag{22}$$

Since v_r is z-dependent only within the characteristic interval $(0, \delta)$, we can approximately write out

$$\frac{\partial v_r}{\partial z} \sim \frac{\partial v_r}{\partial z}\,\Theta(\delta - z),$$

where $z > 0$, and $\Theta(\delta - z)$ is the Heaviside function. The integration of Eqn (22) with respect to z from 0 to H yields

$$\frac{\partial}{\partial t} v_r H \sim \nu \frac{\partial v_r}{\partial z}\bigg|_0^{\delta} \sim \nu \frac{v_r}{\delta}.$$

The multiplication of the last equality by the density ρ and the bottom area S leads us to an equation describing the variation in the radial momentum $\mathcal{P}_r = \rho S H v_r$:

$$\frac{\partial \mathcal{P}_r}{\partial t} \sim \frac{\mathcal{P}_r}{\tau_{sp}}, \qquad \tau_{sp} \sim \frac{H\delta}{\nu} \sim \frac{H}{(\nu\Omega_0)^{1/2}}. \tag{23}$$

Now we estimate the settling times, e.g., for the mode $m = 2$ and for the change in the number of arms due to an abrupt change in the angular velocity at the periphery by $\Delta\Omega$. In the first case ($m = 2$), this time will obviously be longer than $(\tau_{sp})_{min} \approx 0.47$ s: $\tau = \tau_{min}$ at $\Omega = \Omega_1 = 18\ \text{s}^{-1}$ and $H \approx 0.2$ cm (in the central region of the setup, $H > 0.2$ cm). In the second case, for $\Delta\Omega \approx 2\ \text{s}^{-1}$, we have $\tau_{sp} \approx 1.4$ s. The time τ_{in} of developing instability proves to be considerably shorter than these times τ_{sp}: $\tau_{in} \ll \tau_{sp}$. The instability time depends on the velocity spreading in the discontinuity. If this spreading is determined by the molecular viscosity (a laminar Ekman layer), then $\delta_{lam} \sim (\nu/\Omega_1)^{1/2} \approx 2.4 \times 10^{-2}$ cm, i.e., $\delta_{lam} \ll \lambda$, where λ is the radial wavelength ($\lambda \approx 6$ cm for $m = 2$) and $\gamma \approx \Omega_1$ ($\Omega_1 \approx 18\ \text{s}^{-1}$ for $m = 2$), while $\tau_{in} \sim 1/\gamma \approx 5 \times 10^{-2}$ s.

The above-presented arguments for a negligibly weak effect of viscous friction on the excitation of the shear-flow instability in the Spiral' setups are based on experiments with colored water, for which $\nu \approx 0.01\ \text{cm}^2\ \text{s}^{-1}$. It is noted in Ref. [22] that a tenfold increase in the viscosity of the working solution does not qualitatively modify the spiral pattern. The spiral pattern disappears only if the increase in the viscosity is even larger.

A negative answer to the question of the influence of eddy viscosity on pattern formation in the Spiral' setups was given in Ref. [23], where the 'viscous lifetime' of the structures was shown to be completely determined by laminar viscosity.

2.2 A proof of the equivalence between the systems of linearized dynamical equations for a gaseous galactic disk and for rotating shallow water in the Spiral' setups [11]

Since $\tilde{\Psi}$ depends mainly on $\tilde{\sigma}_g$ [11], we write down the system of linearized equations of motion for the gaseous disk of the Galaxy as follows:

$$\frac{\partial v_r}{\partial t} + \Omega_0 \frac{\partial v_r}{\partial \varphi} - 2\Omega_0 v_\varphi = -\frac{\partial}{\partial r}\left(c_{g0}^2\,\eta\right), \tag{24}$$

$$\frac{\partial v_\varphi}{\partial t} + \Omega_0 \frac{\partial v_\varphi}{\partial \varphi} + \frac{\varkappa^2}{2\Omega_0} v_r = -\frac{1}{r}\frac{\partial}{\partial \varphi}\left(c_{g0}^2\,\eta\right), \tag{25}$$

$$\frac{\partial \eta}{\partial t} + \Omega_0 \frac{\partial \eta}{\partial \varphi} + \frac{\partial v_r}{\partial r} + \left(1 + r\ln'\sigma_0\right)\frac{v_r}{r} + \frac{1}{r}\frac{\partial v_\varphi}{\partial \varphi} = 0. \tag{26}$$

Here, the following notation was introduced:

$$\begin{gathered} c_{g0}^2 \equiv c_{s0}^2 - \frac{2\pi G\sigma_0}{|k|R_g}, \qquad c_{s0}^2 \equiv \frac{\mathrm{d}p_0}{\mathrm{d}\sigma_0}, \qquad \eta \equiv \frac{\sigma}{\sigma_0}, \\ \varkappa^2 \equiv 4\Omega_0^2\left(1 + \frac{r}{2}\frac{\Omega_0'}{\Omega_0}\right), \qquad R_g \approx \left(1 + \frac{|k|h}{2}\right)^{-1}; \end{gathered} \tag{27}$$

the prime denotes the differentiation with respect to r; σ is the surface density; k is the wavevector; h is the half-thickness of the gaseous disk, and the stationary quantities are marked with the subscript 0; here, we drop the tildes over the symbols of the perturbed quantities, retaining them from here on only for the amplitudes of the perturbed quantities. When writing down Eqns (24), (25), we used the linearized equation of state

$$\frac{p}{\sigma_0} = c_{s0}^2\,\eta. \tag{28}$$

If we make the substitution

$$c_{g0}^2 = c_{w0}^2 \equiv gH_0, \qquad \eta = \frac{H}{H_0} \tag{29}$$

in Eqns (24)–(26), we arrive at the system of linearized equations of motion of the rotating shallow water [21]. It is such a system that is used to describe small perturbations in shallow water for the Spiral' setups.

The above-presented proof indicates that the setup with rotating shallow water can be used to demonstrate the dynamical structures typical of gaseous galactic disks. Such structures are displayed in Figs 7b–d. The spiral arms rotate clockwise (their ends being directed backward), i.e., the spirals are trailing. Nearly all observed spiral arms of galaxies appear in such a way. The spirals result from a new hydrodynamic instability that we called centrifugal [18]. It was discovered for the first time in the Spiral' setups. The centrifugal instability, like the Kelvin–Helmholtz instability, develops provided a velocity jump is present. However, as shown above, in the case of a supersonic velocity jump, which is present in galactic disks and in the Spiral' setups, the Kelvin–Helmholtz instability is stabilized, and only the new, centrifugal, instability develops. It emerges if a centrifugal force directed outward arises. In this sense, the physics of centrifugal instability is similar to the physics of Rayleigh–Taylor instability which requires the presence of a gravitational force.

2.3 Analytical solution to the system of Eqns (24)–(26) for the case of a tangential discontinuity of the rotational velocity, the sound speed, and surface density [11]

Since the coefficients of the original system of equations (24)–(26) are independent of φ and t, we seek the solution in the form

$$A(r, \varphi, t) = \tilde{A}(r)\exp\left[\mathrm{i}(m\varphi - \omega t)\right]. \tag{30}$$

Then we can reduce equations of motion (24), (25) to a single equation

$$\frac{\mathrm{d}}{\mathrm{d}r}(c_{\mathrm{g}0}^2\tilde{\eta}) = \frac{2m\Omega_0}{r\hat{\omega}}\, c_{\mathrm{g}0}^2\tilde{\eta} + (\hat{\omega}^2 - \varkappa^2)\tilde{\xi}\,, \tag{31}$$

and rewrite equation of continuity (26) as

$$\frac{\mathrm{d}}{\mathrm{d}r}(r\sigma_0\tilde{\xi}) = -r\sigma_0\left[2\,\frac{m\Omega_0}{\hat{\omega}}\,\frac{\tilde{\xi}}{r} + \left(1 - \frac{m^2}{r^2}\,\frac{c_{\mathrm{g}0}^2}{\hat{\omega}^2}\right)\tilde{\eta}\right]. \tag{32}$$

The following notation was used in Eqns (31), (32):

$$v_r \equiv \frac{\mathrm{d}\xi}{\mathrm{d}t} = \left(\frac{\partial}{\partial t} + \frac{v_{0\varphi}}{r}\,\frac{\partial}{\partial\varphi}\right)\xi = -\mathrm{i}\hat{\omega}\xi\,, \qquad \hat{\omega} \equiv \omega - m\Omega_0\,. \tag{33}$$

According to observations of the gaseous disk of the Galaxy (see, e.g., Ref. [24] and references cited therein), an abrupt decline of the rotational curve of the gaseous component occurs near a radius of $R \approx 0.7$ kpc (or, more accurately, at the distances of $R \pm 0.4$ kpc). The distance $R \approx 0.7$ kpc from the center is remarkable in that it is precisely the location of the edge of the central gaseous disk whose surface density $\sigma_{\mathrm{g}1}$ is two orders of magnitude larger than the surface density $\sigma_{\mathrm{g}2}$ of the gas for $r > R$. With further increases in the distance from the center, the surface density of the gas remains virtually constant.

In view of the aforesaid, we will assume that the angular rotational velocity $\Omega_0(r)$, the sound speed $c_{\mathrm{g}0}(r)$, and the surface density $\sigma_0(r)$ of the gas change jumpwise at the distance $r = R$:

$$\begin{aligned}
&\Omega_0(r) = \Omega_1 = \mathrm{const}\,, \quad \sigma_0(r) = \sigma_1 = \mathrm{const}\,,\\
&c_{\mathrm{g}0}(r) = c_{\mathrm{g}1} = \mathrm{const} \quad \text{at} \quad r < R\,;\\
&\Omega_0(r) = \Omega_2 = \mathrm{const}\,, \quad \sigma_0(r) = \sigma_2 = \mathrm{const}\,,\\
&c_{\mathrm{g}0}(r) = c_{\mathrm{g}2} = \mathrm{const} \quad \text{at} \quad r > R\,.
\end{aligned} \tag{34}$$

Integrating Eqns (31) and (32) over the radial layer $(R-\varepsilon,\, R+\varepsilon)$ and letting then $\varepsilon \to 0$ yield the following matching conditions at the discontinuity:

$$(\tilde{\eta}c_{\mathrm{g}0}^2 + R\Omega_0^2\tilde{\xi})_{R-0}^{R+0} = 0\,, \qquad (\tilde{\xi}\sigma_0)_{R-0}^{R+0} = 0\,. \tag{35}$$

Now we reduce the system of two first-order ordinary differential equations (31) and (32) to a single second-order ordinary differential equation. The solution of the latter will contain two arbitrary constants that we will determine from two matching rules (35). The equation being sought will have constant coefficients on both sides of the discontinuity, for $r < R$ and $r > R$. We will employ the latter fact in obtaining this equation.

From Eqn (31), we find that

$$\tilde{\xi} = \frac{c_{\mathrm{g}0}^2}{\tilde{\omega}^2 - \varkappa^2}\left(\frac{\mathrm{d}\tilde{\eta}}{\mathrm{d}r} - \frac{2m\Omega_0}{r\hat{\omega}}\,\tilde{\eta}\right). \tag{36}$$

Next, we substitute the obtained expression for $\tilde{\xi}$ (and the equation for $\tilde{\xi}\,'$, which can straightforwardly be derived) into Eqn (32). After simple manipulations, we arrive at the differential equation for cylindrical functions of the imaginary argument:

$$\tilde{\eta}\,'' + \frac{1}{r}\,\tilde{\eta}\,' - \left(k^2 + \frac{m^2}{r^2}\right)\tilde{\eta} = 0\,, \qquad k^2 \equiv \frac{4\Omega_0^2 - \hat{\omega}^2}{c_{\mathrm{g}0}^2}\,. \tag{37}$$

The general solution of Eqn (37) can be written down in the form [25]

$$\tilde{\eta} = Z_m(\mathrm{i}kr) = C_1 I_m(kr) + C_2 K_m(kr)\,.$$

Since $I_m(x) \to \infty$ as $x \to \infty$, and $K_m(x) \to \infty$ as $x \to 0$, we have the following solutions on the two sides of the discontinuity:

$$\begin{aligned}
&\tilde{\eta}_1 = C_1 I_m(k_1 r)\,, \quad r < R\,;\\
&\tilde{\eta}_2 = C_2 K_m(k_2 r)\,, \quad r > R\,,
\end{aligned} \tag{38}$$

where

$$k_{1,2}^2 \equiv \frac{4\Omega_{1,2}^2 - (\omega - m\Omega_{1,2})^2}{c_{\mathrm{g}1,2}^2}\,.$$

We apply the two matching rules (35) [i.e., we match solutions (38) at $r = R$] to obtain the set of two homogeneous transcendental equations in which the two coefficients of solutions (38) are unknown. The requirement for the solution of this system of homogeneous equations being nontrivial is equivalent to the requirement for the determinant of this system vanishing. As a result, we obtain the following dispersion equation (see the Appendix):

$$k_1^2\alpha_2 - k_2^2\alpha_1 Q\mu^2 + \frac{M^2}{R^2}\,\alpha_1\alpha_2(1 - q^2) = 0\,. \tag{39}$$

Here, we employed the following notation (with the primes designating the differentiation with respect to the argument of the cylindrical function):

$$\begin{aligned}
&\alpha_1 \equiv \frac{2m}{x - m} - k_1 R\,\frac{I_m'(k_1 R)}{I_m(k_1 R)}\,,\\
&\alpha_2 \equiv \frac{2mq}{x - mq} - k_2 R\,\frac{K_m'(k_2 R)}{K_m(k_2 R)}\,,\\
&M \equiv \frac{R\Omega_1}{c_{\mathrm{g}1}}\,, \quad q \equiv \frac{\Omega_2}{\Omega_1}\,, \quad Q \equiv \frac{\sigma_1}{\sigma_2}\,, \quad \mu \equiv \frac{c_{\mathrm{g}2}}{c_{\mathrm{g}1}}\,, \quad x \equiv \frac{\omega}{\Omega_1}\,.
\end{aligned} \tag{40}$$

In terms of the new notation, it follows that

$$\begin{aligned}
&k_1 = \frac{M}{R}\left[4 - (x - m)^2\right]^{1/2},\\
&k_2 = \frac{M}{\mu R}\left[4q^2 - (x - mq)^2\right]^{1/2}.
\end{aligned} \tag{41}$$

The parameter M has the meaning of the Mach number in the neighborhood of the discontinuity (based on the 'inner' velocity, in the region with $r = R - 0$), while q, Q^{-1}, and μ characterize the ratios of the angular velocities, surface densities, and dispersions of the gas velocity in the outer region $(r > R)$ to the corresponding values in the inner region $(r < R)$. Dispersion relation (39) goes over into the dispersion relation of Ref. [26] at $Q = \mu = 1$, because the surface density σ_0 and the dispersion of velocities $c_{\mathrm{g}0}$ were assumed in Ref. [26] to be constant over the entire disk radius and the self-gravitation effects were neglected. As we will show below (see also Ref. [27]), taking into account the jumps in the surface density and in the gas velocity dispersion, along with the jump in the angular velocity, results in finding new physical effects.

2.4 Gradient instabilities at small Mach numbers, $M \ll 1$ [11]

It can be seen from formulas (40) that $k_1 R \sim M \ll 1$ and $k_2 R \sim Mq/\mu$. However, for sufficiently small Mach numbers $M \ll \mu/q$ and for $k_2 R \ll 1$, the expansion of the cylindrical functions $I_m(k_1 R)$ and $K_m(k_2 R)$ in terms of the small argument:

$$\frac{I'_m(k_1 R)}{I_m(k_1 R)} \sim \frac{m}{k_1 R}\,, \qquad \frac{K'_m(k_2 R)}{K_m(k_2 R)} \sim -\frac{m}{k_2 R}\,,$$

yields

$$\alpha_1 = -m\left(1 - \frac{2\Omega_1}{\hat{\omega}_1}\right), \qquad \alpha_2 = m\left(1 + \frac{2\Omega_2}{\hat{\omega}_2}\right);$$

$$\hat{\omega}_{1,2} \equiv \omega - m\Omega_{1,2}\,.$$

Upon substitution of α_1 and α_2 into dispersion relation (39), the latter assumes the form

$$(1+Q)x^2 - 2\big[(m-1) + (m+1)qQ\big]x + m\big[(m-1) + q^2 Q(m+1)\big] = 0\,, \tag{42}$$

with a solution

$$x_{1,2} = (1+Q)^{-1}\Big\{m(1+qQ) + (qQ-1) \pm \mathrm{i}\big[m^2 Q(1-q)^2 - (1-qQ)^2 - m(Q-1)(1+q^2 Q)\big]^{1/2}\Big\}. \tag{43}$$

It is clear why the parameter μ does not appear in dispersion equation (42), where we restricted ourselves to the zeroth order in the expansion in terms of the parameter M. The approximation $M \ll 1$ corresponds to $c_g \to \infty$, irrespective of the factor by which one 'infinity' 'exceeds' the other. The inclusion of the next terms of the expansion in M gives rise to the appearance of μ^2 in the equation; this, however, goes beyond the considered approximation.

Naturally, at $Q = 1$, formula (43) yields the solution obtained in Ref. [26]:

$$x_{1,2} = \frac{1}{2}\Big\{m(1+q) + (q-1) \pm \mathrm{i}\big[(m^2-1)(1-q)^2\big]^{1/2}\Big\}, \qquad Q = 1\,. \tag{44}$$

As can be seen from formula (44), the instability takes place at any $q \neq 1$. This is the Kelvin – Helmholtz instability (KHI); it develops irrespective of which region — outer or inner — rotates more rapidly.

Now consider the case of a solid body rotation of the whole system ($q = 1$) with an arbitrary density gradient $Q \neq 1$. According to Eqn (43), one finds

$$x_{1,2} = (1+Q)^{-1}\Big\{m(1+Q) + (Q-1) \pm \mathrm{i}\big[-(1-Q)^2 + m(1-Q^2)\big]^{1/2}\Big\}, \qquad q = 1\,. \tag{45}$$

It follows from Eqn (45) that, if

$$Q < 1\,, \tag{46}$$

the flute instability (FI) develops, since the outer (denser) layer exerts pressure on the inner (less dense) layer.

Thus, the solution (43) for $q \neq 1$ and $Q < 1$ describes two branches of instability, the KHI and FI. One instability or another can be heightened or weakened by varying the parameters q and Q. For example, the FI can be quenched if the centrifugal force counteracts the gravitational force, i.e., a system with $q < 1$ is prepared. In a similar manner, the KHI can be quenched by the negative density gradient, i.e., by preparing the system with $Q > 1$. An example of such quenching is given below.

Strictly speaking, the KHI and FI cannot be considered separately in the general case. Solution (43) describes the excitation of the shear – flute instability (SFI) or the gradient instability (GI) for $M \ll 1$.

The case of $Q \gg 1$, $q \ll 1$. Let us consider the quenching of the KHI ($q \neq 1$) in the presence of a negative density gradient (i.e., the jump) for $Q > 1$. To see considerable changes, we assume that $Q \gg 1$. To be specific, we choose the parameters q and Q to be typical of our Galaxy: $q \approx 0.1$, and $Q \approx 100$. The results obtained will obviously apply neither to the Galaxy, where $M \gg 1$, nor to other analogous spiral galaxies (I am not aware of the existence of such galaxies with $M \ll 1$).

Thus, we set

$$q \ll 1\,, \qquad Q \gg 1\,, \qquad qQ \gg 1\,, \qquad q^2 Q \sim 1\,. \tag{47}$$

From Eqn (43), in view of the assumptions made in Eqn (47), we find

$$x_{1,2} = q(m+1) \pm \mathrm{i}Q^{-1/2}\big[m^2(1-q)^2 - (m-1)q^2 Q - m\big]^{1/2}, \tag{48}$$

so that the instability condition is written down as

$$m^2(1-q)^2 > (m+1)q^2 Q + m \tag{49}$$

or, for $q \ll 1$, as

$$q^2 Q < \frac{m-1}{m+1}\,m\,. \tag{50}$$

According to inequality (50), instability is not possible at $m = 0$, 1; instability with $m = 2$ develops on condition that $q^2 Q < 2/3$, and so forth.

Thus, a large negative density gradient stabilizes the system. From formula (48), we find the azimuthal phase velocity of the disturbance wave:

$$\Omega_{\mathrm{ph}} \equiv \frac{\omega}{m} = \frac{m+1}{m}\,\Omega_2\,, \qquad Q \gg 1\,, \qquad Qq \gg 1\,. \tag{51}$$

For comparison, we write out the same quantity at $Q = 1$ [26]:

$$\Omega_{\mathrm{ph}} = \frac{\Omega_1 + \Omega_2}{2} - \frac{\Omega_1 - \Omega_2}{2m}\,, \qquad Q = 1\,. \tag{52}$$

The difference in the phase velocities is not significant at small m (and $q \ll 1$); for example, at $m = 2$, one has

$$\frac{(\Omega_{\mathrm{ph}})_{Q \gg 1}}{(\Omega_{\mathrm{ph}})_{Q=1}} \equiv \alpha_{\mathrm{ph}} \approx 6q\,,$$

which amounts to $\alpha_{\mathrm{ph}} \approx 0.6$ at $q \approx 0.1$.

However, as known from theoretical [26] and experimental [18 – 20] studies, if $M \ll 1$, modes with large $m \gg 1$ are generated. For $m \gg 1$, the difference in the phase velocities is more significant:

$$\frac{(\Omega_{\mathrm{ph}})_{Q \gg 1}}{(\Omega_{\mathrm{ph}})_{Q=1}} \equiv \alpha_{\mathrm{ph}} \approx 2q\,.$$

If $q \approx 0.1$, the difference in the phase velocities reaches 5, i.e., $\alpha_{ph} \approx 0.2$. Thus, the density wave with $Q \gg 1$ (and $q \ll 1$) rotates with a smaller azimuthal velocity than does the same wave with $Q = 1$ (and $q \ll 1$). Accordingly, the corotation radius in the case of $Q \gg 1$ is larger than that at $Q = 1$.

2.5 Gradient instabilities at large Mach numbers, $M \gg 1$ [11]

We represent x as $x_1 + iMx_2$ to obtain from Eqn (41):

$$k_1 \approx \frac{M^2 x_2}{R} - i\,\frac{M}{R}(x_1 - m)\,, \tag{53}$$

$$k_2 \approx \frac{M^2 x_2}{\mu R} - i\,\frac{M}{\mu R}(x_1 - mq)\,. \tag{54}$$

Substituting k_1 and k_2 into the dispersion equation (39), we obtain

$$x_1 = \frac{m(1 + Q\mu q)}{1 + Q\mu}\,, \qquad x_2 = \frac{1 - q^2}{1 + Q\mu}\,, \tag{55}$$

or

$$x = (1 + Q\mu)^{-1}\left[m(1 + Qmq) + iM(1 - q^2)\right]. \tag{56}$$

In the particular case of $Q = \mu = 1$, expression (56) goes over into solution [26]

$$x = \frac{1}{2}\left[m(1 + q) + iM(1 - q^2)\right], \qquad Q = \mu = 1\,, \tag{57}$$

which differs substantially from solution (44) in that it indicates the instability only for $q < 1$, while the latter describes the instability at any $q \neq 1$. Therefore, for $M \gg 1$, the instability develops only if the inner part of the system, $r < R$, rotates with a higher angular velocity than does the outer part. We designated this instability as the centrifugal instability (CI) [18–20]. The physics of this instability is similar to the mechanism of developing flute instability and substantially differs from the physics of the KHI. The stabilization of the KHI for two-dimensional disturbances with the proviso that $M > 2\sqrt{2}$ was proved in Ref. [8].

In the particular case of the solid body rotation of the whole system ($q = 1$), we find from formula (56) that

$$x = (1 + Q\mu)^{-1}\, m(1 + Qm)\,, \qquad q = 1\,. \tag{58}$$

Now let us determine the azimuthal phase velocity of the disturbances in the general case described by the solution

$$\Omega_{ph} = \frac{\mathrm{Re}\,\omega}{m} = \frac{1 + Q\mu q}{1 + Q\mu}\,\Omega_1\,. \tag{59}$$

Note that in the particular case of $Q = \mu = 1$ [26] one has

$$\Omega_{ph} = \frac{\mathrm{Re}\,\omega}{m} = \frac{1 + q}{2}\,\Omega_1\,. \tag{60}$$

In the Galaxy, it is believed that $q \approx 0.1$, $Q \approx 100$, and $\mu \sim 0.1$,[4] i.e., we obtain from formula (59) the following result:

$$(\Omega_{ph})_{Gal} \approx \frac{0.36\,\Omega_1}{2}\,. \tag{61}$$

This means that the corotation radius is considerably larger than that predicted by the theory for $Q = 1$ [26],

$$(\Omega_{ph})_{Gal} \approx \frac{\Omega_1}{2}\,, \qquad Q = 1\,. \tag{62}$$

The velocities Ω_{ph} given by formulas (61) and (62) differ by a factor of about three. The value of Ω_{ph} measured in the experiments [18–20] was several times smaller than Ω_{ph} given by formula (60) [26]. Estimates show that the Ω_{ph} values calculated according to formula (59) are similar to those measured in the experiments [18–20]. The Ω_{ph} value obtained from formula (61) for the Galaxy agrees better with modern estimates [28] of the quantity Ω_{ph} than the value taken from formula (62).

Now we determine the shape of the spiral pattern generated by the CI beyond the discontinuity radius (in the region with $r > R$). For the perturbed density σ in the region with $r > R$, we find from formulas (38), taking into account formula (54), that

$$\sigma \propto K_m(k_2 r)\exp(im\varphi) \propto r^{1/2}\exp\left\{-\frac{\Omega_1^2 R r}{c_{g1}c_{g2}}\,\frac{1 - q^2}{1 + Q\mu} + im\left[\varphi + \frac{\Omega_1 r}{c_{g2}}\,\frac{1 - q}{1 + Q\mu}\right]\right\}. \tag{63}$$

Two conclusions can be extracted from solution (63):

(1) the necessary condition for the finiteness of the solution coincides with the condition of development of the CI for $M \gg 1$;

(2) the density waves appear as trailing spirals only in the system with the angular rotational velocity decreasing with an increase in radius, i.e., for $q < 1$. The last condition is necessary for the development of the CI in the system.

The radial wavelength can easily be determined from relationship (63) to be

$$\lambda_r = \frac{2\pi}{k_r} = 2\pi\,\frac{c_{g2}}{\Omega_1 m}\,\frac{1 + Q\mu}{1 - q}\,. \tag{64}$$

3. Appendix

The substitution of $\tilde{\eta}$ from formulas (38) into Eqn (36) with the use of the notation introduced in formulas (40) yields the following expressions for $\tilde{\xi}_1$ and $\tilde{\xi}_2$ that refer to the regions with $r < R$ and $r > R$, respectively:

$$\tilde{\xi}_1 = C_1\,\frac{\alpha_1 I_m}{k_1^2 R}\,, \quad r < R\,; \qquad \tilde{\xi}_2 = C_2\,\frac{\alpha_2 K_m}{k_2^2 R}\,, \quad r > R\,. \tag{65}$$

Based on the second matching rule (35), we write down the relationship

$$C_1\,\frac{\sigma_1\alpha_1}{k_1^2}\,I_m = C_2\,\frac{\sigma_2\alpha_2}{k_2^2}\,K_m\,. \tag{66}$$

From the first matching rule (35), we find

$$\tilde{\eta}_1 + \frac{M^2}{R}\,\tilde{\xi}_1 = \mu^2\tilde{\eta}_2 + \frac{M^2 q^2}{R}\,\tilde{\xi}_2 \tag{67}$$

[4] In the Galaxy, at $r = R$ (i.e., at $r \approx 0.7$ kpc), the quantities $c_{g0}^2 \approx c_{s0}^2$ and μ are completely determined by the equation of state. For a polytropic model with $(p/\sigma^{\gamma_{pl}}) = \mathrm{const}$ $\mu = Q^{(1-\gamma_{pl})/2}$ and at $\gamma_{pl} \approx 2$, we have $\mu \approx Q^{-1/2}$. This means that $\mu = 0.1$ (at $Q = 100$); in the molecular disk, this corresponds to a turbulent velocity of $c_{s,\,turb} \approx 80$ km s^{-1}. If, however, we substitute the non-self-consistent value of $(c_{s,\,turb})_{min} \approx 20$ km s^{-1} into formula (59), we will obtain in formula (61) that $\Omega_{ph} \approx 0.26\,\Omega_1/2$ instead of $0.36\,\Omega_1/2$. The difference is obviously insignificant.

or, using relationships (38) and (65), we arrive at

$$\left(1 + M^2 \frac{\alpha_1}{k_1^2 R^2}\right) I_m C_1 = \left(\mu^2 + M^2 q^2 \frac{\alpha_2}{k_2^2 R^2}\right) K_m C_2 . \quad (68)$$

The system of homogeneous transcendental equations (66) and (68) has a nontrivial solution for the unknown functions C_1 and C_2 determined from the condition of the zero determinant of this system. The last condition comes to be equivalent to the dispersion equation (39) that is being sought.

4. Theoretical prediction and experimental confirmation of superreflection instability in the rotating shallow water setup

4.1 Historical background

Theoretical studies of the problem of reflection of a monochromatic acoustic wave from a plane–parallel tangential discontinuity of velocity, accompanied by wave amplification, were pioneered by Miles [29] and Ribner [30]. It was found that, if the velocity of the moving medium is sufficiently high, the wave incident normally upon the discontinuity from the motionless medium can be reflected with amplification. In this process, the amplitude of the reflected wave becomes larger than the amplitude of the incident wave. This is due to the fact that a negative-energy wave (or, more precisely, a quasienergy wave [31]) goes to the moving medium, while a positive-energy wave goes to the motionless medium. This wave, emitted to the motionless medium, replenishes its energy from the moving medium [32]. For the development of the instability, an acoustic feedback must be added — for example, a wall forcing the wave reflected from the tangential discontinuity of velocity to return to the discontinuity, being amplified again.

Another amplification mechanism for the reflected wave is the resonant amplification of the acoustic wave that occurs if the tangential discontinuity of velocity is slightly smoothed out to a thin, finite-width shear layer [33]. In this case, a thin critical layer appears within the shear region, and the energy of the acoustic wave grows in this layer. Therefore, an additional branch of unstable oscillations can arise due to the interaction with resonance particles [32].

Thus, if a reflecting wall is present, a superreflection instability can develop. However, the Kelvin – Helmholtz instability (of the tangential discontinuity) can simultaneously be excited in the same system with a plane – parallel tangential discontinuity of velocity; similarly, a centrifugal instability can also occur in a system with a cylindrical tangential discontinuity of velocity (in a two-dimensional axisymmetric flow). As a rule, the last two hydrodynamic instability mechanisms are more powerful than the superreflection instability. Therefore, the superreflection instability can be revealed only in the absence of these stronger instabilities.

The hydrodynamic medium in which the superreflection instability was investigated constitutes a layer of rotating shallow water with a free surface. It is known [7] that the dynamics of such a medium can be described by two-dimensional equations equivalent to the corresponding equations of motion of a two-dimensional compressible medium. In this case, wave perturbations of the layer depth (surface gravity waves) in shallow water correspond to wave perturbations of the surface density in a two-dimensional compressible medium, and the role of the speed of sound in the shallow-water case is played by the propagation velocity of the gravity waves.[5]

A theoretical stabilization criterion for the Kelvin – Helmholtz instability of a moving two-dimensional compressible fluid with plane – parallel tangential discontinuity of velocity was obtained for the first time by Landau [8]. According to this criterion, if only a velocity jump is present, there is no tangential-discontinuity instability, provided the Mach number obeys the inequality

$$M \geqslant 2\sqrt{2} . \quad (69)$$

Here, $M \equiv |\Delta V|/c_s$, $|\Delta V|$ is the magnitude of the velocity jump in the flow, and c_s is the sound speed in the gas. This criterion was experimentally verified (to within the experimental errors) for layers of rotating shallow water [34].

Another hydrodynamic instability should be excited in a moving two-dimensional compressible fluid with cylindrical tangential discontinuity of velocity, with the inner part of fluid rotating more rapidly than the outer one at a sufficiently high Mach number [with condition (69) satisfied]. This instability, which came to be known as centrifugal instability [18], was experimentally investigated using the Spiral' setup with rotating shallow water [15, 18].

In an opposite case, namely

$$\Omega_1 < \Omega_2 , \quad (70)$$

where Ω_1 and Ω_2 are the angular rotational velocities of the inner and outer parts of the shallow water, respectively, and if condition (69) is satisfied, both instabilities (i.e., the tangential discontinuity instability and the centrifugal instability) are quenched.

Some remarks are in order here. On the one hand, theoretical and numerical analyses are limited in this case to the linear approximation. On the other hand, we would like to apply our results to the nonlinear structures actually generated in the experimental setup. In which cases is this admissible? In general, the amplitude of the structures [wave patterns formed by the perturbations of the shallow-water-layer depth $h(r, \varphi, t)$[6]] that we predict for the experiment is not small: $|h| \sim \mathcal{O}(H_0)$, where H_0 is the unperturbed depth of the layer; however, the horizontal size of these structures is large, i.e., $|k_\perp h| \ll 1$ (where $|k_\perp h| = |\nabla_\perp h|$), and the variations in the surface height are assumed to be fairly smooth. For the applicability of the linearized model, the condition $|k_\perp h| \ll 1$ is not sufficient, and we assume in addition that $|h| \ll H_0$. For this reason, we conjecture that, if a linear unstable perturbation mode is detected (corresponding, at a given set of unperturbed parameters, to axisymmetric, steadily rotating shallow water) and its growth rate is considerably larger than that of other possible unstable modes, it is precisely this mode that will be generated in the experimental setup at the given

[5] Two-dimensional compressible media should be distinguished from three-dimensional compressible media. Shallow water belongs to the first class. As is known, water is not compressible in the three-dimensional case, and its continuity equation reduces to $\operatorname{div} \mathbf{v} = 0$. At the same time, shallow water is described by the two-dimensional continuity equation for a compressible fluid: $\partial\sigma/\partial t + \operatorname{div}(\sigma \mathbf{v}) = 0$.

[6] We use a cylindrical coordinate system r, φ, z, which is natural in this case; the unperturbed flow is assumed to be axisymmetric.

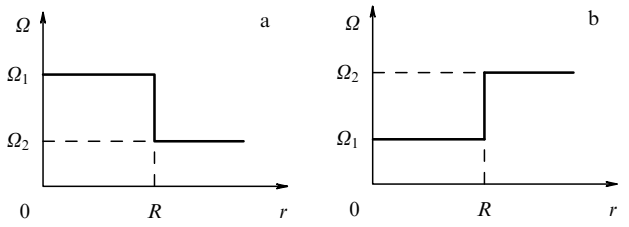

Figure 8. The rotation curve in the cases with (a) and without (b) a centrifugal instability.

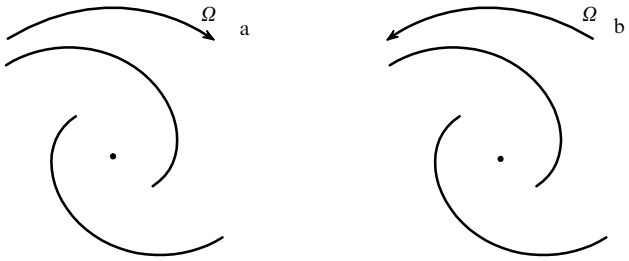

Figure 9. Schematic of trailing (a) and leading (b) spiral waves. The arrows indicate the directions of rotation of the shallow water.

parameters. The results of previous theoretical considerations and laboratory experiments concerning the Kelvin–Helmholtz and the centrifugal instabilities in the system at hand confirmed that, for sufficiently unstable modes, the spiral–vortex structures calculated using a linear model agree well with the nonlinear stationary structures observed at the experimental setup [18–20, 15].

The centrifugal instability develops at any large Mach number provided that the angular rotational velocity Ω_1 of the central (inner with respect to the velocity jump) part exceeds the angular rotational velocity Ω_2 at the periphery, i.e., $\Omega_1/\Omega_2 > 1$.

Such velocity jumps (Fig. 8a) are observed in the disks of half the spiral galaxies [35–38].

The physics of centrifugal instability is similar to that of Rayleigh–Taylor instability typical of the situation where a denser fluid overlies another fluid in a gravitational field. In the case of centrifugal instability, the centrifugal force in the central part of the rotating system is larger than at the periphery; similarly, in Rayleigh–Taylor instability, the gravitational force acting on the denser fluid is larger than that acting on the less dense fluid.

The centrifugal instability generates trailing spiral waves rotating so that the spiral ends are directed backward [18–20]. Therefore, these waves have a good 'aerodynamic' shape (Fig. 9a). The larger the velocity jump $\Delta\Omega$, the less the number m of trailing spiral waves generated by the centrifugal instability [18–20].

4.2 Theoretical prediction of superreflection instability in rotating shallow water. A schematic of the setup [39, 40]

The shear layer is a source of hydrodynamic instabilities. Among them, the Kelvin–Helmholtz and the centrifugal instability are the strongest ones. However, they can be quenched if the parameters of the setup are properly chosen.

For simplicity, we will mainly consider a flow with only one discontinuity in the rotation curve $\Omega_0(r)$, assuming $\Omega_0(r) = \Omega_1$ for $r < R$, and $\Omega_0(r) = \Omega_2$ for $r > R$ (Fig. 8b). Let us set

$$0 \leqslant \bar{q} = \frac{\Omega_1}{\Omega_2} < 1\,. \tag{71}$$

In this case, the centrifugal instability will be quenched.

In a real experiment, because of viscous spreading, a transition layer with a characteristic width $\sim 2H_0$, where H_0 is the layer depth, forms near the velocity jump. This depth is assumed to be small compared to all characteristic scales of the problem. Thus, to comprehend the situation on a qualitative level, it is sufficient to analyze the sharp discontinuity in the rotation curve (we will discuss the effects of the finite width of the velocity jump in the next section).

The velocity jump at the discontinuity is characterized by the Mach number

$$M \equiv R\,\frac{\Omega_2 - \Omega_1}{c_{s0}}\,, \tag{72}$$

where c_{s0} is the sound speed. By analogy with a plane velocity jump, the Kelvin–Helmholtz instability in rotating shallow water is quenched for $M \geqslant M_{cr}$. Our numerical analysis shows that, in contrast to the plane shear layer where $M_{cr} = 2\sqrt{2}$, we have $2 < M_{cr} < 2\sqrt{2}$ for a cylindrical tangential discontinuity. In this case, the exact stability boundary varies slightly with a number m of the azimuthal mode. In what follows, we assume that the Mach number is large enough to quench the Kelvin–Helmholtz instability.

The dispersion relation for the instability analysis of the shear layer in shallow water with a free surface can be obtained from the linearized hydrodynamic equations describing an inviscid medium [11]:

$$\begin{aligned}
&\frac{\partial v_r}{\partial t} + \Omega_0\,\frac{\partial}{\partial\varphi}\,v_r - 2\Omega_0 v_\varphi = -\frac{\partial}{\partial r}(c_{s0}^2\eta)\,,\\
&\frac{\partial v_\varphi}{\partial t} + \Omega_0\,\frac{\partial}{\partial\varphi}\,v_\varphi + \frac{\varkappa^2}{2\Omega_0}\,v_r = -\frac{1}{r}\,\frac{\partial}{\partial\varphi}(c_{s0}^2\eta)\,,\\
&\frac{\partial\eta}{\partial t} + \frac{1}{rH_0}\,\frac{\partial}{\partial r}(rH_0 v_r) + \frac{1}{r}\,\frac{\partial}{\partial\varphi}(\eta\Omega_0 r + v_\varphi) = 0\,,
\end{aligned} \tag{73}$$

where v_r and v_φ are the radial and azimuthal velocities, respectively; H_0 is the depth of the shallow water (assumed to be constant); $\eta = h/H_0$ is the normalized perturbation of the depth; $\Omega_0(r)$ is the angular rotational velocity, and $\varkappa$ is the epicyclic frequency: $\varkappa(r) = (4\Omega_0^2 + r\,\mathrm{d}\Omega_0^2/\mathrm{d}r)^{1/2}$. The role of the sound speed c_{s0} is played by the propagation velocity of long gravitational waves: $c_{s0} = (gH_0)^{1/2}$, where g is the gravitational acceleration. We will seek the general solution in the form

$$f(r,\varphi,t) = \mathrm{Re}\left[\sum_m \int f(r)\exp\left[\mathrm{i}(m\varphi - \omega t)\right]\mathrm{d}\omega\right], \tag{74}$$

where $\omega = \mathrm{Re}\,\omega + \mathrm{i}\,\mathrm{Im}\,\omega$. In the framework of the linear approximation (since we are interested in studying 'linear' instability), we can use the superposition principle, considering separately an mth ($m \geqslant 1$) harmonic.

In the case of an arbitrary, continuous rotation curve and an arbitrary profile of the sound speed, the system of differential equations (73) can be reduced to the following

equations [11]

$$\frac{\mathrm{d}}{\mathrm{d}r}(c_{s0}^2\eta) = \frac{2m\Omega}{r\hat{\omega}}\, c_{s0}^2\eta - (\varkappa^2 - \hat{\omega}^2)\xi\,,$$
$$\frac{\mathrm{d}}{\mathrm{d}r}(rH_0\xi) = -rH_0\left[\left(1 - \frac{m^2c_{s0}^2}{r^2\hat{\omega}^2}\right)\eta + \frac{2\,m\Omega_0}{r\hat{\omega}}\,\xi\right] \tag{75}$$

with corresponding boundary conditions. Here, $\xi(r)$ is the perturbed radial Lagrangian displacement defined according to the equality $v_r = -\mathrm{i}\hat{\omega}(r)\xi(r)$, with $\hat{\omega} = \omega - m\Omega_0$.

In the case of a sharp discontinuity in the rotation curve (Fig. 8b), the relative perturbations of the shallow water depth on both sides of the discontinuity can be represented by Bessel functions:

$$\eta(r) = C_1 H_m^{(1)}(kr) + C_2 H_m^{(2)}(kr)\,, \tag{76}$$

where $H_m^{(1,2)}$ are the Hankel functions of the first and second kinds. The analog of the radial wavenumber k depends on the perturbation frequency ω:

$$k^2 = \frac{\hat{\omega}^2 - 4\Omega_0^2}{c_{s0}^2}\,. \tag{77}$$

Since the rotation curve represents a piecewise constant function, the wavenumbers on both sides of the jump are also constant (we denote them as k_1 and k_2 for the inner and the outer regions, respectively). For simplicity, we assume that the inner wall is located at $R_a = 0$, and the outer wall is directed to infinity: $R_b \to \infty$.

From the boundary conditions and the matching conditions at the tangential discontinuity, we can obtain the dispersion equation [11]

$$\alpha_1\left[(x-1)^2 - \frac{4}{m^2}\right] - \alpha_2\left[(x-\bar{q})^2 - \frac{4\bar{q}^2}{m^2}\right] + \alpha_1\alpha_2\,\frac{\bar{q}^2 - 1}{m^2} = 0\,, \tag{78}$$

where

$$\alpha_1 = \frac{2\bar{q}}{x-\bar{q}} - k_1R\,\frac{J_m'(k_1R)}{J_m(k_1R)}\,, \quad \alpha_2 = \frac{2}{x-1} - k_2R\,\frac{H_m'^{(1)}(k_2R)}{H_m^{(1)}(k_2R)}\,.$$

Here, $J_m'(z)$ and $H_m'^{(1)}(z)$ are the derivatives of the functions $J_m(z)$ and $H_m^{(1)}(z)$ with respect to r, and the dimensionless eigenfrequency $x = \omega/(m\Omega_2)$ was introduced.

The eigenfrequencies of interest are solutions of this dispersion relation, and the wavenumbers k_1 and k_2 can be found from these solutions.

If the real part of the wavenumber is much larger than the imaginary part, eigenfunction (76) describes a solution in the form of a wave. In the opposite case, the eigenfunction increases or decreases exponentially.

It can be found from Eqn (77) that k_1 is real provided that

$$\mathrm{Re}\,x > \bar{q}\left(1 + \frac{2}{m}\right), \tag{79}$$

while k_2 is real provided that

$$\mathrm{Re}\,x < 1 - \frac{2}{m}\,. \tag{80}$$

These considerations suggest a qualitative classification of modes according to their behavior in the inner and outer (with respect to the velocity jump) regions. We will distinguish three different cases depending on whether k_1 and k_2 are real or imaginary.

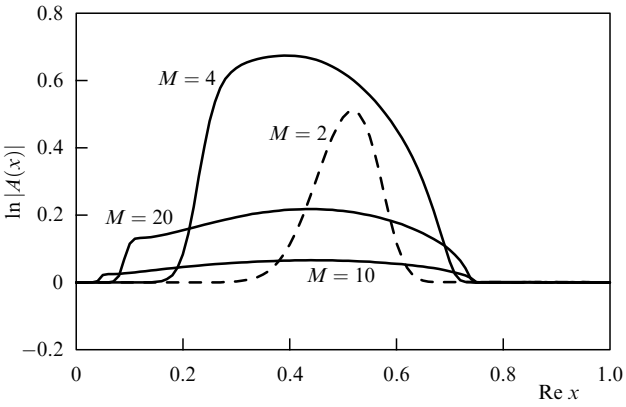

Figure 10. Logarithm of the magnitude of the reflection coefficient, $\ln|A(x)|$, as a function of $\mathrm{Re}\,x$ at $m = 8$, $\bar{q} = 0$, and various Mach numbers M. If $M = 4.2$, the maxima of the curves decrease with M at any azimuthal mode number m. Note that in the case of a cylindrical tangential discontinuity the amplification is already possible for $M > 1$ (while for a plane–parallel discontinuity, only for $M > 2$).

(1) *Type I modes*: *k_1 and k_2 are real*. In this case, the solutions on both sides of the Ω_0 jump are of a wave character. This is possible for azimuthal wavenumbers

$$m > \frac{2}{1 - \mathrm{Re}\,x}\,. \tag{81}$$

In view of the fact that $\bar{q} < \mathrm{Re}\,x < 1$ for unstable modes, inequality (81) implies that the minimum number of arms in unstable wave patterns of this type is $m = 3$.

Consider the case of $\bar{q} = 0$. The wave in the inner part propagates between the left-hand wall (placed at the origin where $r = 0$) and the Ω_0 jump. Under certain conditions, this wave reflects from the discontinuity with an amplitude larger than the amplitude of the incident wave (superreflection), in complete analogy with the Miles – Ribner effect (Fig. 10).

If feedback is applied, this gives rise to the unstable solutions reported by Kolykhalov [41] for a planar geometry. The number of unstable modes can be large. The real parts of the eigenfrequencies can be determined from the equation

$$J_m'(k_1R) = 0\,. \tag{82}$$

Since k_1R has an order of magnitude of the large parameter Mm, the number of modes of this type is of an order of Mm/π.

If $x_n^{(0)}$ are the roots of equation (82), the eigenfrequencies can be described by the approximate formula

$$\frac{x_n}{x_n^{(0)}} = 1 - \frac{1}{M^2} + \mathrm{i}\,\frac{m}{M^3}\left[\left(1 - x_n^{(0)}\right)^2 - \frac{4}{m^2}\right]^{1/2}. \tag{83}$$

(2) *Type II modes*: *k_1 is real, and k_2 is imaginary*. A wave-type solution exists in the inner region, and an exponential solution in the outer region. This occurs if $\mathrm{Re}\,x > 1 - 2/m$. For these frequencies, however, the inner wave cannot be amplified at the discontinuity, as follows from Fig. 10.

Nevertheless, numerical computations indicate that one mode of this type exists for any $m \geqslant 1$. As the Mach number is

varied gradually, this mode becomes alternately neutral and unstable.

The real part of the frequency for $M \gg m \gg 1$ is approximately equal to

$$x_0 = 1 - \frac{1}{M} + \frac{2{,}25}{M^2} + \ldots . \tag{84}$$

The maximum of the imaginary frequency is of an order of the following magnitude:

$$\max \operatorname{Im} x \sim \frac{1 - x_0}{M} \sqrt{2x_0} \sim \frac{1}{M^2} \sqrt{2x_0} . \tag{85}$$

(3) *Type III modes*: k_1 *is imaginary, and* k_2 *is real*. An exponential solution exists in the inner region, and a wave-type solution in the outer region. This situation is possible only if $\bar{q} > 0$ and $\operatorname{Re} x < \bar{q}(1 + 2/m)$.

It can be shown analytically that one mode of this type exists for azimuthal numbers $m \geqslant 3$. The approximate equations for the real and the imaginary parts of x are fairly awkward, and we do not present them here in an explicit form. The real part is close to the limit placed at $x_0 = \bar{q}(1 + 2/m)$. The imaginary part in the limiting case of $M \gg m \gg 1$ is of order

$$\operatorname{Im} x \sim \bar{q} \frac{2}{M^3} \sqrt{m^2 - 4} . \tag{86}$$

Unstable modes of this type are of an emissive nature, i.e., they grow due to the emission of negative energy to infinity.

Analytical and numerical calculations for moderate M and m values

$$2.2 < M < 6 , \qquad m < 10 , \tag{87}$$

indicate that the growth rates of the type-I and type-II modes are comparable, while the growth rates of the type-III modes are much smaller. For this reason, type-III modes could hardly be revealed in experiments. As for the first two types, their growth rates will be maximum if $|\Omega_2 - \Omega_1|$ is at the most, i.e., if $\bar{q} = \Omega_1/\Omega_2 = 0$. Thus, from here on, we will consider the case of $\Omega_1 = 0$.

Taking into account the presence of the outer boundary of the system at $r = R_b$ modifies the dispersion equation (78), and its numerical solution indicates that, at sufficiently large Mach numbers, unstable solutions (corresponding to the superreflection instability) can emerge for any azimuthal mode with $m \geqslant 1$. At any given m, these solutions correspond to either type I or type II.

A typical behavior of the unstable roots that refer to the superreflection instability with varying Mach number, at a given m, is shown in Fig. 11. The letter A labels the solutions corresponding to type-II modes, and the letter B labels the most unstable solutions corresponding to type-I modes (with a nearly exponential damping of the amplitude in the inner region, from the Ω_0 jump to the center). The subscripts on A and B specify the number of maxima of the radial function $\eta(r)$ in the wave zone (for A, in the inner part, and for B in the outer part). This means, in particular, that the unstable solution A_2 is a type-II mode with two nodes along the spiral arm in the inner part.

The dependence shown in Fig. 11 reveals a resonant behavior of unstable eigenfrequencies corresponding to the superreflection instability. For this reason, various modes can be observed in an experiment as the Mach number is varied.

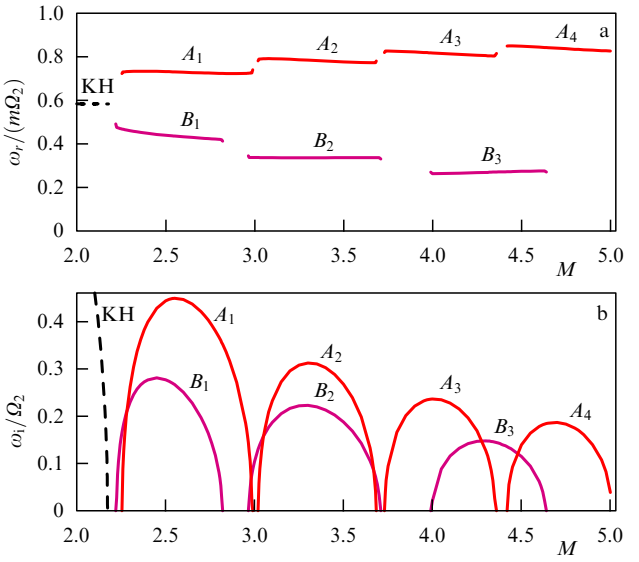

Figure 11. The Mach-number dependence of the dimensionless eigenfrequencies at $m = 5$ as obtained from the numerical solution of Eqn (78) modified for the case where inner and outer rigid walls at radii of $0.04R$ and $1.7R$ are introduced into the system: (a) normalized real part of the frequency, i.e., the angular phase velocity of the generated spiral structure, and (b) normalized imaginary part of the frequency, i.e., the growth rate of disturbances: A_j, type-II unstable mode; j, the number of nodes in the wave region (in the inner part); B_k, type-I unstable mode; k, the number of nodes in the outer region; KH (the dashed curves in the left-hand parts of the graphs), the unstable Kelvin – Helmholtz mode.

4.3 A scheme of experiment on the laboratory modeling of superreflection instability

Consider a realistic model of the rotating shear layer. The parameters of this model should be carefully adjusted so as to satisfy certain physical requirements and maximize the growth rate of the superreflection instability, which should dominate over viscous damping and dispersive spreading. In this case, the optimal parameters could be used in designing the experimental setup for studies of the superreflection instability.

We suggest the geometry of the experimental setup shown in Fig. 12. It consists of two parts, one being placed inside the other. The inner part is a motionless horizontal disk of radius R_{in}. The outer part is a conical surface of inner radius R_{in} and outer radius R_{out}. In the experiment considered, the lengths of the waves generated on the shallow-water surface should exceed by several times the capillary wavelength for water (1.73 cm) in order for surface tension effects to be negligible.

While the outer part is rotating, a small amount of water is poured into the container so that the fluid forms a thin layer

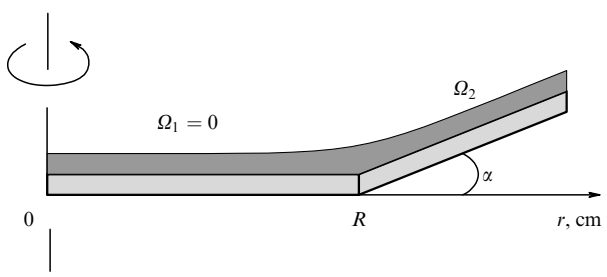

Figure 12. The geometry of the experiment.

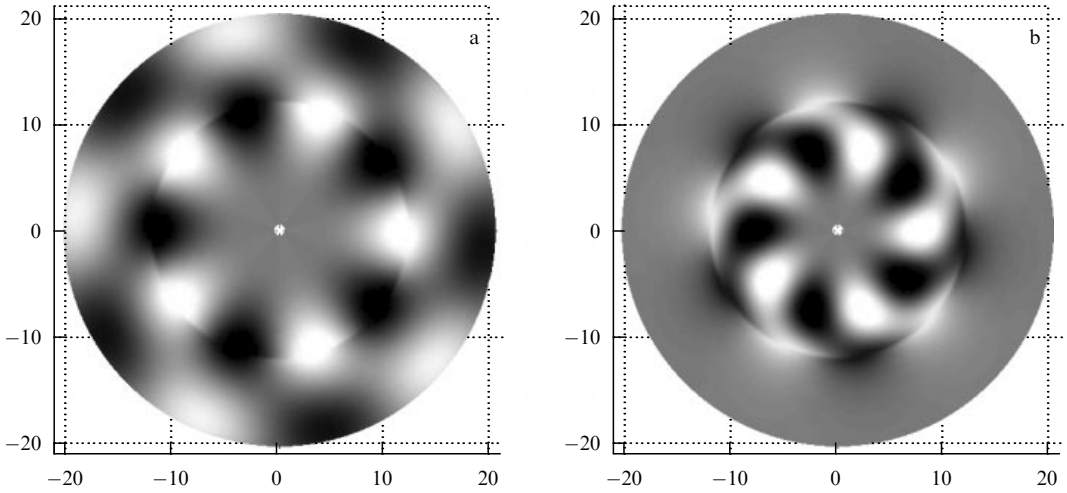

Figure 13. Unstable five-armed type-I modes B_1 (a) and type-II modes A_1 (b) obtained by numerically solving the eigenvalue problem (75). The Mach number is $M = 2.7$.

covering the surfaces of both parts of the bottom. The depth of the water layer is a few millimeters. It must be several times larger than the depth of the Ekman layer [21] but sufficiently small to keep the shallow water approximation applicable [7].

The bottom profile of the outer part should be chosen so that the shallow water depth is as close to uniformity as possible. In reality, the undisturbed free surface for $r > R$ is nearly paraboloidal. However, the shape of the paraboloid depends on the angular velocity of the outer part. Therefore, the constancy condition can be strictly satisfied for the shallow water depth only at a certain value of the angular velocity. If the velocity jump is fixed, the Mach number can be changed only by varying the shallow water depth. However, this technique is less convenient than alteration of the rotational velocity. Therefore, we suggest a constant inclination of the outer part of the bottom ($\alpha_0 \approx 15^\circ$) at which the water depth can be considered nearly constant in the Mach number range $2.2 < M < 6.0$.

The velocity shear layer in the proposed experimental setup is not infinitely narrow. Therefore, the effect of the velocity jump smoothing out on the generation mechanism of unstable modes must be considered. Thus, in addition to the sharp discontinuity, we analyzed a small viscous spreading of the jump:

$$\Omega(r) = \frac{\Omega}{2}\left(1 + \tanh\frac{r-R}{L}\right), \tag{88}$$

where L is the width of the tangential discontinuity smoothing, $L \leqslant H_0$.

Such a dynamical system can be analyzed numerically. Instead of solving the dispersion relation, an eigenvalue problem should be solved for system (75) with corresponding boundary conditions.

The basic result of these computations lies in the fact that the weak smoothing of the above-considered tangential discontinuity reduces the growth rates of the unstable solutions, i.e., the superreflection instability weakens. However, the growth rates still remain large enough for the superreflection instability being manifest in the experiment. Given the Mach number, modes differing in their type and azimuthal number can have closely spaced growth rates. Nevertheless, as the Mach number is increased, a monotonic decrease in the number m of arms of the most unstable mode can be observed (if the increase in the Mach number is achieved by increasing the angular rotational velocity Ω at the periphery).

The wave patterns obtained in our numerical simulations for the rotation curve given by formula (88) are demonstrated in Figs 13–15. In all cases, we put $L = H_0/2$. The rotational direction of the patterns and the periphery is counterclockwise.

Figure 13 displays two patterns with five arms that can form as superreflection instability develops at a Mach number of $M = 2.7$.

The three- and four-armed patterns of unstable modes that can develop due to superreflection instability at $M = 2.8$ are shown in Fig. 14.

For comparison, the patterns of three-armed unstable Kelvin – Helmholtz and superreflection modes are presented in Fig. 15.

Thus, our investigation revealed that the superreflection instability generates structures with wave patterns of the types illustrated in Figs 13b, 14b, and 15b. These large-scale structures are leading spirals (Fig. 9b) generated by the region of the smoothed rotational velocity jump.

For a fixed azimuthal harmonic number m, the Mach number dependences of the growth rates of two basic (type-I and type-II) families of unstable superreflection roots are of a resonant nature (see Fig. 11).

Since the growth rate maxima sharply decrease with an increase in the Mach number, the range recommended for the experimental investigation of the superreflection instability is $2.2 < M < 4.5$. In view of the velocity jump smoothing out to halfwidths of $L \sim H_0/2$, the small scale structures ($m \gtrsim 8$) turn out to be stabilized. As the Mach number is increased in this range, mode restructuring (according to their maximum increments) from $m \sim 6, 7$ via $(m-1), (m-2), \ldots$, up to $m = 3, 4$ can be observed.

The wave patterns formed with the development of the superreflection instability differ from those generated by the Kelvin – Helmholtz instability (Fig. 15a). The latter are virtually radial structures that damp monotonically on both sides of the velocity discontinuity.

In addition, the wave patterns excited by the superreflection instability differ from those patterns that are set

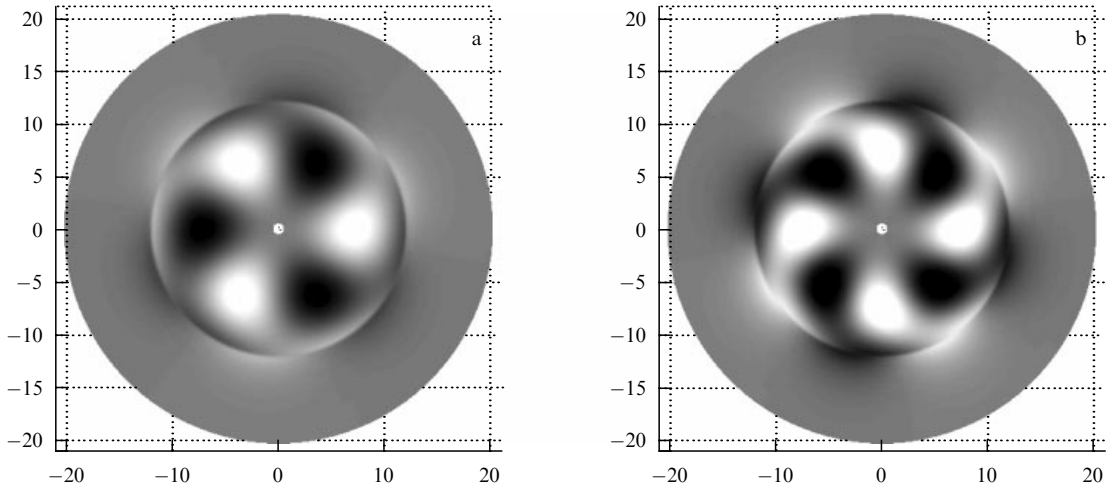

Figure 14. Three-armed (a) and four-armed (b) unstable type-II modes (A_1). The Mach number is $M = 2.8$.

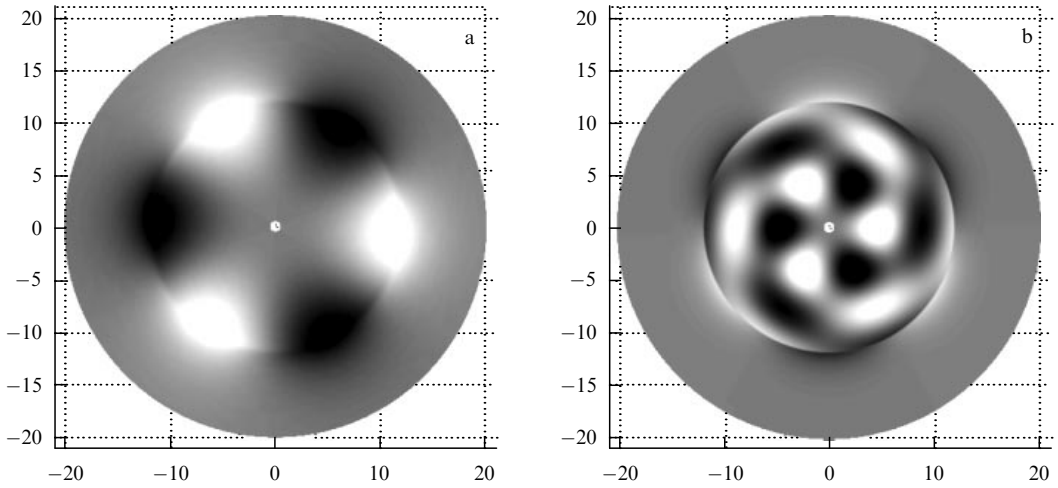

Figure 15. Unstable three-armed Kelvin – Helmholtz modes for a Mach number $M = 2.0$ (a) and superreflection (A_2) type-II modes for a Mach number $M = 4.2$ (b).

by centrifugal instability. The latter generates trailing (Fig. 9a), tightly twisted spirals localized near the velocity jump. The centrifugal mechanism can be triggered only if the radial decrease in the angular velocity of rotation is sufficiently rapid (more rapid than by the $\sim r^{-2}$ law near the jump).

4.4 Experimental discovery of superreflection instability in the rotating shallow water setup [42]

As described above, a smooth layer with a free surface overlies a differentially rotating bottom. The original equations of two-dimensional hydrodynamics, describing the evolution of the surface layer of the fluid, are presented in a monograph by Pedlosky [21]. The sound speed in these equations corresponds to the quantity $(gH)^{1/2}$, where g is the free fall acceleration, and H is the depth of the fluid layer. The angular velocity of rotation increases as the radius increases, thus quenching the strong centrifugal instability [18]. Another mechanism that could prevent carrying out the experiment is the instability of the tangential discontinuity of velocity. Virtually, the latter cannot develop in a supersonic regime, where precisely the superreflection instability is possible. If the condition $\Omega_2 > \Omega_1$ (where Ω_1 and Ω_2 are the angular velocities of rotation in the central and peripheral parts, respectively) is satisfied for the setup, the competing centrifugal instability cannot develop either [18]. At the same time, this condition does not prevent the development of the superreflection instability.

Our experiments were carried out using the setup shown in Fig. 16. A thin layer of fluid covered the bottom of a container that resembled a frying pan. The outer part of the bottom rotating at the angular velocity Ω_0 was conical (the angle being 15°). The inner part of the bottom was motionless, so that $\Omega_0 = 0$. The mechanical interaction of the fluid with the bottom was ensured by the rotational forces with a sharp velocity jump in the zone between the corresponding parts of the layer — the outer 'periphery' with an outer diameter of $D = 41$ cm, and the inner 'core'.

The setup was equipped with a black-and-white video camera. To record the field of the layer depth perturbations, we used the optical densitometry method which works well if the bottom is white [15, 43]. The fluid was simply green-colored water, so that the thickening of the layer, as viewed through a red light filter, appeared darker than the regions of

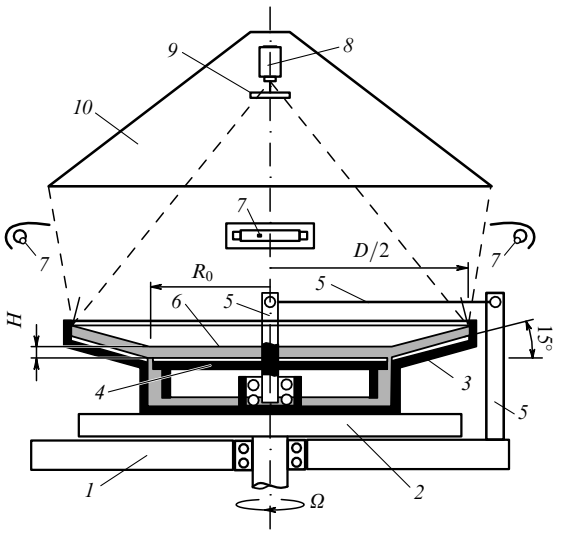

Figure 16. Schematic of the setup: *1*, motionless plate; *2*, table rotating with the angular velocity Ω_0; *3*, rotating container with a conical bottom; *4*, plane motionless part of the bottom; *5*, axial column of diameter 8 mm submerged into the fluid layer; *6*, layer of the greenish fluid (with a free surface); *7*, white halogen lamps; *8*, black-and-white camera; *9*, red light filter; *10*, black diffusing shield.

smaller surface densities. The relative perturbations in the experiments were less than 20%.

The experiment was started with a stationary regime in which the fluid layer completely covered the bottom and was made as thin as possible. The core remained motionless, while the periphery rotated as a solid body. We decreased the Mach number $M = \Omega_0 R_0/(gH)^{1/2}$ very slowly, reducing the rotational velocity Ω_0 or adding fresh fluid to the container and thus increasing the layer thickness H. (The quantity H was measured near the center of the core.) At a certain $M_0 \equiv M(R_0)$, the layer thickness became perturbed in the circular zone in the core, which is adjacent to the rotating periphery. The perturbations emerged at the periphery in the form of nearly radial 'spokes' varying in their length and width along the azimuth, depending on the rotational velocity. Some time later, even if M_0 remained unchanged, disorder emerged in the previously stable single structure (wave pattern) rotating in the same direction at the constant angular velocity $\Omega_{\rm ph}$. This structure, having an m-order rotational symmetry, definitely exhibited the development of a hydrodynamic instability with the azimuthal number m (a typical structure with $m = 6$ is shown in Fig. 17a; structures with different numbers m are also developing). As M_0 was further decreased, the system came again to order, and kindred structures with progressively larger m appeared again. As the number M_0 increased, we observed reverse transitions to structures with progressively smaller m. Both transitions — with decreasing and increasing M_0 — exhibited signs of a hysteresis, obviously attesting that the nonlinearity of the observed structures showed its worth. The wavenumbers of the observed modes varied from 3 to 10. The modes emerging at their stability – instability thresholds could be successfully controlled. The number of modes depended on many factors, such as the prehistory, the law of time variations in M_0, the way in which the fluid was added, the viscosity, etc. Notice that modes 5 and 6 proved to be the most stable in the face of variations in the conditions. Other characteristics varied similarly to the variations in centrifugal instability [18], $\Omega_{\rm ph}$ decreased with decreasing Ω_0 and increasing m. At sufficiently small M_0, the system was brought into the zone where a predominant role was played by the tangential-discontinuity (Kelvin – Helmholtz) instability characterized by the development of azimuthal modes with $m = 1$ and 2.

To identify the observed instability, let us try to compare the structure shown in Fig. 17b with the theoretically evaluated eigenfunction of the superreflection instability [39, 40] for physical conditions close to those of the experiment (Fig. 17a). The eigenfunction appears as a superposition of two coherent systems. In turn, each system consists of six leading spiral waves moving outward, toward the velocity shear. At a certain distance from the shear, the waves moving

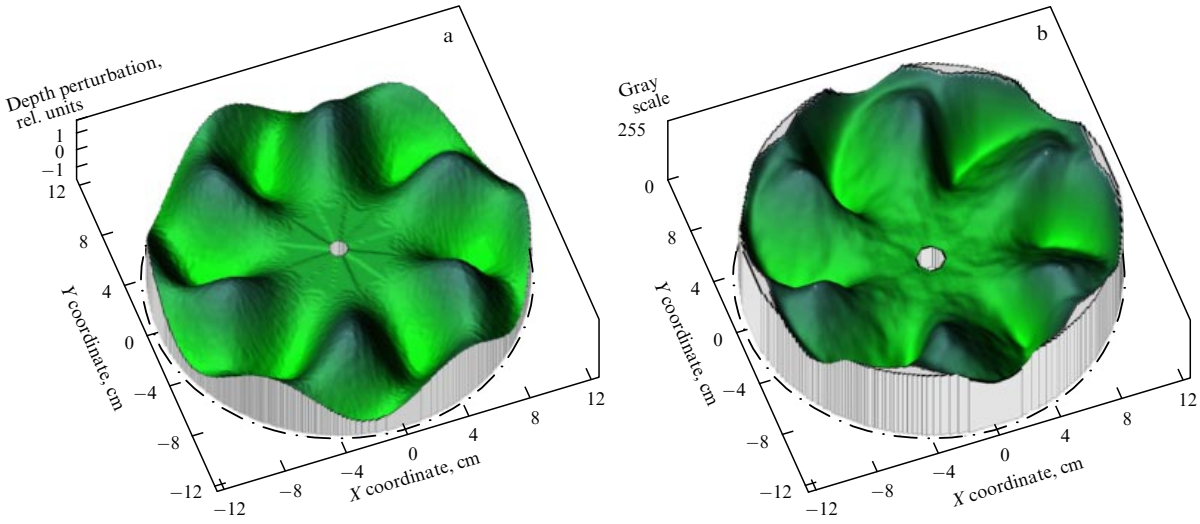

Figure 17. Typical structures relevant to the mode $m = 6$ generated by the superreflection instability. (a) Theoretically evaluated eigenfunction in the process of development of the superreflection instability [39, 40] [$H = 5.0$ mm, $\Omega_0 = 4.83$ rad s^{-1} ($M_0 = 2.62$), $\Omega_{\rm ph} = 4.25$ rad s^{-1} ($M_{\rm ph0} = 2.30$), the characteristic width of the shear region is close to H]. The rotation is directed clockwise. (b) The disturbance of the fluid layer thickness in an experiment [42] expressed in arbitrary units [$H = 4.0$ mm, $\Omega_0 = 3.98$ rad s^{-1} ($M_0 = 2.4$), $\Omega_{\rm ph} = 3.13$ rad s^{-1} ($M_{\rm ph0} = 1.9$)]. Good agreement between experimental and theoretical results can be noted.

inward prove to be more intense than those moving outward. This agrees exactly with the theoretical predictions [39, 40]. The similarity between the graphs is remarkable, especially in view of the fact that the *a priori* results for nonlinear structures affected by viscosity as they are generated were compared with the *de facto* results of the linear inviscid theory.

Acknowledgments

I sincerely appreciate the valuable help from my colleagues S G Poltorak, E V Polyachenko, and Yu M Torgashin in preparing this review article. This work was supported by the Russian Foundation for Basic Research (project No. 05-02-17874a), the State Program for Support to Leading Scientific Schools of the Russian Federation (grant NSh-7629.2006.2), and the basic-research program Extended Objects in the Universe of the Physical Sciences Division of the Russian Academy of Sciences (project Collective Processes and Structures in Astrophysical Disks).

References

1. Helmholtz H *Philos. Mag.* **36** 337 (1868)
2. Kelvin W *Philos. Mag. 5* **24** 188 (1887)
3. Rayleigh Lord *Proc. Math. Soc. London Ser. A* **93** 148 (1916)
4. Taylor G I *Philos. Trans. R. Soc. London Ser. A* **223** 289 (1923)
5. Lamb H *Hydrodynamics* 6th ed. (Cambridge: The Univ. Press, 1932) [Translated into Russian (Moscow – Leningrad: Gostekhizdat, 1947)]
6. Sedov L I *Mekhanika Sploshnoi Sredy* (A Course in Continuum Mechanics) Vols 1, 2, 2nd ed. (Moscow: Nauka, 1973) [Translated into English (Groningen: Wolters-Noordhoff, 1971)]
7. Landau L D, Lifshitz E M *Gidrodinamika* (Fluid Mechanics) (Moscow: Nauka, 1986) [Translated into English (Oxford: Pergamon Press, 1987)]
8. Landau L D *Dokl. Akad. Nauk SSSR* **44** 151 (1944) [*C.R.* (*Dokl.*) *Acad. Sci. USSR* **44** 151 (1944)]
9. Syrovatskii S I *Zh. Eksp. Teor. Fiz.* **27** 121 (1954)
10. Fridman A M *Usp. Fiz. Nauk* **160** (10) 179 (1990) [*Sov. Phys. Usp.* **33** 865 (1990)]
11. Fridman A M *Zh. Eksp. Teor. Fiz.* **98** 1121 (1990) [*Sov. Phys. JETP* **71** 627 (1990)]
12. Loitsyanskiy L G *Mekhanika Zhidkosti i Gaza* (Mechanics of Liquids and Gases) (Moscow: Nauka, 1973) [Translated into English (New York: Begell House, 1995)]
13. Gor'kavyi N N, Fridman A M *Fizika Planetnykh Kolets*: *Nebesnaya Mekhanika Sploshnoi Sredy* (The Physics of Planetary Rings: Celestial Mechanics of Continuous Media) (Moscow: Nauka, 1994)
14. Fridman A, Gor'kavyi N *Physics of Planetary Rings*: *Celestial Mechanics of Continuous Media* (New York: Springer-Verlag, 1999)
15. Nezlin M V, Snezhkin E N *Rossby Vortices, Spiral Structures, Solitons*: *Astrophysics and Plasma Physics in Shallow Water Experiments* (Berlin: Springer-Verlag, 1993)
16. Morozov A G, Fainshtein V G, Fridman A M *Dokl. Akad. Nauk SSSR* **228** 1072 (1976)
17. Mikhailovskii A B *Teoriya Plazmennykh Neustoichivostei* (Theory of Plasma Instabilities) Vol. 2, 2nd ed. (Moscow: Atomizdat, 1977) p. 31 [Translated into English: Vol. 2 (New York: Consultants Bureau, 1974)]
18. Fridman A M et al. *Phys. Lett. A* **109** 228 (1985)
19. Morozov A G, Nezlin M V, Snezhkin E N, Fridman A M *Pis'ma Zh. Eksp. Teor. Fiz.* **39** 504 (1984) [*JETP Lett.* **39** 613 (1984)]
20. Morozov A G, Nezlin M V, Snezhkin E N, Fridman A M *Usp. Fiz. Nauk* **145** 161 (1985) [*Sov. Phys. Usp.* **28** 101 (1985)]
21. Pedlosky J *Geophysical Fluid Dynamics* (New York: Springer-Verlag, 1979) [Translated into Russian (Moscow: Mir, 1984)]
22. Nezlin M V et al. *Zh. Eksp. Teor. Fiz.* **92** 3 (1987) [*Sov. Phys. JETP* **65** 1 (1987)]
23. Antipov S V et al. *Fiz. Plazmy* **14** 1104 (1988) [*Sov. J. Plasma Phys.* **14** 648 (1988)]
24. Sumin A A, Fridman A M, Haud U A *Pis'ma Astron. Zh.* **17** 698 (1991) [*Sov. Astron. Lett.* **17** 295 (1991)]
25. Jahnke E, Emde F, Lösch F *Tafeln höherer Funktionen* (Stuttgart: Teubner, 1960) [Translated into English: *Tables of Higher Functions* (New York: McGraw-Hill, 1960); Translated into Russian (Moscow: Nauka, 1964)]
26. Morozov A G *Pis'ma Astron. Zh.* **3** 177 (1977)
27. Fridman A M, in *Dynamics of Astrophysical Discs* (Ed. J Sellwood) (Cambridge: Cambridge Univ. Press, 1989) p. 185
28. Fridman A M *Usp. Fiz. Nauk* **177** 121 (2007) [*Phys. Usp.* **50** 115 (2007)]
29. Miles J W *J. Acoust. Soc. Am.* **29** 226 (1957)
30. Ribner H S *J. Acoust. Soc. Am.* **29** 435 (1957)
31. McIntaier M E *J. Fluid Mech.* **106** 454 (1981)
32. Stepanyants Yu A, Fabrikant A L *Usp. Fiz. Nauk* **159** 83 (1989) [*Sov. Phys. Usp.* **32** 783 (1989)]
33. Blumen W, Drazin P G, Billings D F *J. Fluid Mech.* **71** 305 (1975)
34. Antipov S V et al. *Pis'ma Zh. Eksp. Teor. Fiz.* **37** 319 (1983) [*JETP Lett.* **37** 378 (1983)]
35. Afanasiev V L et al. *Astrofiz.* **28** 243 (1988) [*Astrophys.* **28** 142 (1988)]
36. Afanasiev V L et al. *Astrofiz.* **29** 155 (1988) [*Astrophys.* **29** 497 (1988)]
37. Afanasev V L et al. *Astron. Zh.* **68** 1134 (1991) [*Sov. Astron.* **35** 569 (1991)]
38. Afanasev V L et al. *Astron. Zh.* **69** 19 (1992) [*Sov. Astron.* **36** 10 (1992)]
39. Fridman A M et al., in *Astrophysical Disks*: *Collective and Stochastic Phenomena* (Astrophysics and Space Science Library, Vol. 337, Eds A M Fridman, M Ya Marov, I G Kovalenko) (Dordrecht: Springer-Verlag, 2006) p. 3
40. Fridman A M et al. *Phys. Lett. A* **349** 198 (2006)
41. Kolykhalov P I *Izv. Akad. Nauk SSSR Mekh. Zhidk. Gaza* (3) 145 (1984)
42. Fridman A M et al. *Phys. Lett.* (in press)
43. Rylov A Yu, Snezhkin E N, Titishov K B *Astron. Zh.* **81** 306 (2004) [*Astron. Rep.* **48** 275 (2004)]